Article

The International Journal of Robotics Research
2014, Vol. 33(12) 1569–1592

DOI: 10.1177/0278364914537130
ijr.sagepub.com

Trajectory tracking with collision avoidance for nonholonomic vehicles with acceleration constraints and limited sensing

Erick J. Rodríguez-Seda[1], Chinpei Tang[2], Mark W. Spong[3] and Dušan M. Stipanović[4]

Abstract

Nowadays, autonomously operated nonholonomic vehicles are employed in a wide range of applications, ranging from relatively simple household chores (e.g. carpet vacuuming and lawn mowing) to highly sophisticated assignments (e.g. outer space exploration and combat missions). Each application may require different levels of accuracy and capabilities from the vehicles, yet, all expect the same critical outcome: to safely complete the task while avoiding collisions with obstacles and the environment. Herein, we report on a bounded control law for nonholonomic systems of unicycle-type that satisfactorily drive a vehicle along a desired trajectory while guaranteeing a minimum safe distance from another vehicle or obstacle at all times. The control law is comprised of two parts. The first is a trajectory tracking and set-point stabilization control law that accounts for the vehicle's kinematic and dynamic constraints (i.e. restrictions on velocity and acceleration). We show that the bounded tracking control law enforces global asymptotic convergence to the desired trajectory and local exponential stability of the full state vector in the case of set-point stabilization. The second part is a real-time avoidance control law that guarantees collision-free transit for the vehicle in noncooperative and cooperative scenarios independently of bounded uncertainties and errors in the obstacles' detection process. The avoidance control acts locally, meaning that it is only active when an obstacle is close and null when the obstacle is safely away. Moreover, the avoidance control is designed according to the vehicle's acceleration limits to compensate for lags in the vehicle's reaction time. The performance of the synthesized control law is then evaluated and validated via simulation and experimental tests.

Keywords

Motion control, wheeled robots, distributed robot systems, collision avoidance, control of nonholonomic systems

1. Introduction

Unmanned nonholonomic vehicles have attracted lot of interest from scientific, industrial, and governmental sectors. Nowadays, autonomous nonholonomic vehicles are used in several applications including the exploration of outer space bodies (Bogue, 2012), the sampling of atmospheric and oceanic conditions (Leonard et al., 2007), the handling of materials in warehouses (Wurman et al., 2008), and the recognition of targets in conflict and disaster zones (Cole et al., 2009). Their future is also very promising as advances in electronic, computation, control, and communication keep extending the vehicles' capabilities and, consequently, their potential applications. Yet, the use of unmanned nonholonomic vehicles may still, to this day, pose several control challenges. From a theoretical perspective, the nonholonomic property implies: (a) that not every direction of motion for the vehicle is admissible and (b) that there is no smooth time-invariant state feedback control law capable of asymptotically stabilizing the system (Brockett, 1983). Furthermore, from a practical perspective, the reliance on actuators and embedded sensors with limited capabilities may negatively affect the accomplishment of a task as well as the vehicle's safety (Kumar and Michael, 2012). For instance, vehicles' motors are subjected to friction forces and saturated control torques that limit their maximum achievable acceleration and velocity and, consequently, their maneuverability. Similarly, onboard proximity sensing mechanisms used for navigation and collision avoidance, such as computer-based vision systems and sonar radars, may exhibit low resolution, large sampling times, and measurement noises that can compromise the vehicle's safety by misestimating the distance

[1]Weapons and Systems Engineering, United States Naval Academy, Annapolis, MD, USA
[2]Caterpillar Global Mining Division, Denison, TX, USA
[3]School of Engineering and Computer Science, University of Texas, Dallas, TX, USA
[4]Coordinated Science Laboratory, University of Illinois, Urbana, IL, USA

Corresponding author:
Erick J. Rodríguez-Seda, United States Naval Academy, Weapons and Systems Engineering, 105 Maryland Ave, Annapolis, MD 21402, USA.
Email: rodrigue@usna.edu

to nearby obstacles. Therefore, in order to keep up with the accelerated pace of technology and the unfolding of applications for unmanned vehicles, several of these control challenges must be tackled.

In this paper, we will focus on the design of control solutions for nonholonomic vehicles (specifically, differential two-wheel drive robots with rolling without slipping condition, also refer to as unicycle-type) considering both dynamic constraints and limited sensing capabilities. We will first address the trajectory tracking and set-point stabilization problem of a nonholonomic vehicle taking into account the saturation of the control torques and velocities. Then, we will address the collision avoidance problem when the vehicle's sensing range is bounded and the position of obstacles and other nearby agents is uncertain.

1.1. Related work

1.1.1. Feedback control of nonholonomic systems. Nonholonomic vehicles present control challenges atypical to holonomic systems. Brockett's theorem (1983) implies that a nonholonomic system cannot be asymptotically stabilized to a single equilibrium point by the use of a smooth static (Bloch and McClamroch, 1989; Campion et al., 1991) (or even dynamic (D'Andréa Novel et al., 1995)) time-invariant state feedback control. Consequently, full-state feedback linearization and the use of conventional linear control tools cannot be directly applied. To solve this limitation and still achieve exponential or, at least, asymptotic stability of the full-state system, several other control ideas have been proposed including time-variant state feedback control laws (Pomet, 1992; Samson, 1995; Do et al., 2004), discontinuous control strategies (Canudas de Wit and Sørdalen, 1992; Astolfi, 1996; Aguiar et al., 2000), and hybrid control techniques (Pomet et al., 1992; Sørdalen and Egeland, 1995). Alternatively, many researchers have opted for the partial asymptotic stabilization of the vehicle rather than the full state representation. That is the case of input–output feedback linearization methods that allow the use of conventional linear analysis (Sarkar et al., 1994; Yamamoto and Yun, 1994; Lawton et al., 2003). Another control approach based on the construction of transverse functions is presented in work by Morin and Samson (2009) which guarantees the practical stabilization of the nonholonomic system to any desired trajectory. By practical stabilization it is meant that the state errors are arbitrarily ultimately bounded. In Kolmanovsky and McClamroch (1995), several other control solutions are discussed.

In addition to the challenges inhered from the vehicle's nonholonomic nature, there exist control problems derived from physical and practical limitations. For instance, the saturation of the motors' control torque and the effects of friction may impose a bound on the vehicle's velocity and acceleration. This means that the vehicle might not be able to reach a desired position or trajectory in an arbitrary short time, much less to instantaneously change its direction of motion. Yet, conventional control solutions for nonholonomic vehicles are typically based on kinematic models that assume direct control of the vehicle's velocity or on dynamic models with unconstrained acceleration and control torque (Kolmanovsky and McClamroch, 1995; Loizou and Kyriakopoulos, 2008). Both formulations imply that the vehicle can reach any point in space arbitrarily fast and change its direction of motion almost instantaneously. To correctly account for velocity limitations, a backstepping control law for dynamic controllers considering velocity constraints is proposed in Loizou and Kyriakopoulos (2008). Similarly, feedback control laws with bounded velocities applied to kinematic models have been reported in Oriolo et al. (2002), Consolini et al. (2008), and Oikonomopoulos et al. (2009). These control solutions, however, are built under the assumption of unlimited actuation. To account for control torque limitations, Canudas de Wit and Roskam (1991) introduced a path-following control law in which feasible paths are constructed in accordance with input torque constraints. However, the generation of these feasible paths does not necessarily verify the application of control inputs with predefined bounds. Alternatively, Lawton et al. (2003) proposed a bounded input–output feedback linearization control strategy that guarantees set-point stabilization of a nonholonomic vehicle taking into account limited actuation. Their control formulation was applied to the static formation of multiple vehicles and validated via experimental results. Yet, the authors do not provide an analytical bound for the control laws. Finally, Chen *et al.* (Chen et al., 2012) recently reported a bounded, continuous, time-varying controller that achieves semiglobal stabilization of a unicycle-type vehicle with control bounds and parameters that depend on the initial state of the system.

1.1.2. Collision avoidance. Another control challenge in the operation of unmanned vehicles is to verify the safety of the system and to maintain collision-free trajectories at all times. Unmanned vehicles are frequently expected to share the space with other agents[1] and/or to operate in unknown, cluttered environments. Hence, the vehicle must be embedded with a sensing mechanism capable of estimating the position of nearby agents and with an avoidance strategy to avoid collisions according to such estimates. Furthermore, sensing mechanisms may be subjected to measurement errors such as errors due to delays, noise, low-resolution, and disconnections (see Moravec, 1988; John A Volpe National Transportation Systems Center, 2001; Kinsey et al., 2006; Rodríguez-Seda et al., 2011a, for more discussion on the topic), requiring the collision avoidance policy to compensate for these uncertainties.

Collision avoidance strategies for nonholonomic vehicles can be designed from two paradigms: motion planning control (i.e. open-loop) and reactive control (i.e. closed-loop). In a motion planning strategy, the controller determines a collision-free trajectory that the vehicle must follow based

on the estimated position of obstacles at an initial sampling time. Since the estimates must remain valid through the entire trajectory (i.e. obstacles must not diverge significantly from their initial position), fast moving obstacles, including other vehicles, must not be present in the vehicle's environment. Conversely, a reactive strategy, also known as real-time, computes the control inputs online as obstacles are detected facilitating the interaction with dynamic obstacles. Therefore, reactive collision avoidance strategies are preferred when working in dynamic environments. Reactive collision avoidance laws for nonholonomic systems with unconstrained acceleration and velocity have been proposed in Mastellone et al. (2008) and Palafox and Spong (2009) for kinematic models and in De La Cruz and Carelli (2008), Do (2008), Do (2009), and Kowalczyk et al. (2010) for dynamic models. Similarly, reactive collision avoidance for vehicles with bounded velocities are reported in Lalish et al. (2008); Rodríguez-Seda (2014) for kinematic models and in Loizou and Kyriakopoulos (2008) for dynamic models. A heuristic motion planning with collision avoidance strategy for vehicles with bounded velocity and acceleration is proposed in Snape et al. (2011) with no rigorous guarantee of their success. Another control approach that takes into account the saturation of the control inputs is presented in Lalish and Morgansen (2012), where the authors introduce a reactive, distributed avoidance algorithm based on the concept of velocity obstacles (Fiorini and Shiller, 1998). Finally, in Lamiraux et al. (2004), a collision-free path planning algorithm is developed for kinematic models that deforms the vehicle's desired path online as obstacles are detected. Their work guarantees collision-free transit for nonholonomic robots without velocity or acceleration bounds.

The aforementioned collision avoidance strategies assume near perfect obstacle sensing, that is, the acquisition of accurate obstacle position information. Previous work on collision avoidance explicitly considering sensing errors include probabilistic-based methods (Moravec, 1988; Elfes, 1989; Fulgenzi et al., 2007) and the use of control techniques based on reachable sets (Frew and Sengupta, 2004). These methods, however, are exclusively formulated for static or time-constant velocity obstacles. Extensions to dynamic obstacles with acceleration constraints are presented in Althoff et al. (2012), where a control probabilistic approach is reported for vehicles with double integrator dynamics. Their work stems from the notion of inevitable collision states (Fraichard and Asama, 2003). Similarly, in Rodríguez-Seda et al. (2011a), reactive collision avoidance strategies are proposed for pairs of double integrators. The work in Rodríguez-Seda et al. (2011a), which builds on the concept of avoidance control (Leitmann and Skowronski, 1977), analytically guarantees collision-free trajectories under constrained actuation (i.e. bounded acceleration and velocity) as well as sensor uncertainties. An akin, yet, more conservative approach with similar considerations is presented in Rodríguez-Seda et al. (2011b); Rodríguez-Seda and Spong (2012) for multiple vehicles with nonlinear Lagrangian dynamics.

1.2. Contributions

In this paper, we report on a trajectory tracking control law with collision avoidance for nonholonomic vehicles of unicycle type that considers both dynamic and kinematic constraints along with limited sensing capabilities. First, we develop a bounded control solution for the trajectory tacking and set-point stabilization problem taking into consideration the wheels' velocity and acceleration constraints. Then, we synthesize the tracking control law with a reactive collision avoidance strategy designed to accommodate for obstacle detection errors (e.g. errors due to delays, noise, and quantization) as well as limited sensing range. The trajectory tracking control law follows a similar approach to Lawton et al. (2003), where bounded input–output feedback linearization is employed, but tailored herein to the trajectory tracking problem and offering analytical bounds on the vehicle's admissible velocity and acceleration. Moreover, the proposed control law is shown to achieve global asymptotic convergence to the desired trajectory and local exponential stability of the full state vector in the case of set-point stabilization. The collision avoidance strategy, on the other hand, follows the approach presented in Rodríguez-Seda et al. (2011a) which is inspired by the concept of avoidance control (Leitmann and Skowronski, 1977). The avoidance strategy is reactive or real-time, meaning that control inputs are computed online as obstacles are detected as opposed to motion planning-based strategies. Furthermore, the avoidance control strategy takes into consideration kinematic and dynamic constraints, is arguably easy to implement (it does not required the computation of reachable sets as well as solutions to Hamilton–Jacobi partial differential equations), and is shown to be robust to obstacle detection errors. In addition, the proposed avoidance control law is exclusively active when other obstacles are close. This implies that the vehicle can follow the desired trajectory without perturbations when obstacles are safely away. The overall control law is validated via the use of Lyapunov-based analysis and its performance illustrated via simulation and experimental tests.

1.3. Organization

The paper is organized as follows. Section 2 models the kinematic and dynamic equations of motion for a nonholonomic two-wheel drive vehicle and introduces the control objectives. The nonlinear equations of motion and control torque bounds are presented in Section 2.1, while the input–output linearized model is developed in Section 2.2. Section 3 formulates the bounded tracking control law for a single vehicle and demonstrates closed-loop stability and convergence of the vehicle's position to a time-varying desired trajectory or a set-point. In Section 4, we define the collision

avoidance problem for a pair of two agents, namely the *i*th and *j*th agents, which could represent a pair of vehicles or a vehicle and an obstacle. To differentiate properties and signals between both agents, we append the subscripts i and j to the notation. Section 4.2 develops the bounded avoidance control law, whereas Section 4.3 establishes sufficient conditions for collision avoidance under sensing uncertainties for the noncooperative (when only one vehicle implements the avoidance control) and cooperative (when both vehicles implement an avoidance strategy) cases. Boundedness of the overall control law is proven in Section 5. Finally, simulation results with two static obstacles and a pair of vehicles are presented in Section 6, while experimental results with a pair of nonholonomic iRobot Create robots are illustrated and discussed in Section 7.

2. Problem formulation

2.1. Vehicle dynamics

In this paper, we aim to develop control strategies for nonholonomic two-wheel drive vehicles (see Figure 1) satisfying the rolling without slipping condition. The kinematic and dynamic equations of motion for the vehicle are given by

$$\begin{bmatrix} \dot{x}(t) \\ \dot{y}(t) \\ \dot{\phi}(t) \\ \dot{v}(t) \\ \dot{\omega}(t) \end{bmatrix} = \begin{bmatrix} v(t)\cos\phi(t) \\ v(t)\sin\phi(t) \\ \omega(t) \\ \frac{1}{\rho m}(\tau_R(t)+\tau_L(t)) \\ \frac{l}{\rho J}(\tau_R(t)-\tau_L(t)) \end{bmatrix} \tag{1}$$

where $[x(t), y(t)]^{\mathrm{T}} = \mathbf{z}^c(t)$ are the Cartesian coordinates of the center of inertia (assumed to coincide with the axle's midpoint), $\phi(t)$ is the angular orientation or heading, $v(t)$ is the linear velocity, $\omega(t)$ is the angular velocity, $\tau_L(t)$ and $\tau_R(t)$ are the applied control torques for the left and right wheels, respectively, ρ is the wheels' radius, l is the distance between both wheels, and m and J are the mass and moment of inertia, respectively. We consider the practical case in which the control torques are subjected to saturation, i.e. $-M_L \leq \tau_L(t) \leq M_L$ and $-M_R \leq \tau_R(t) \leq M_R$ for $t \geq 0$ and some $M_L, M_R > 0$, which also implies that the vehicle's acceleration signals are bounded. Without loss of generality, we assume that $M_L = M_R = M > 0$. Furthermore, we take the control inputs to be computed according to

$$\begin{aligned} \tau_R(t) &= \frac{\rho m}{2}(f(t)-kv(t)) + \frac{\rho J}{2l}(\tau(t)-k\omega(t)) \\ \tau_L(t) &= \frac{\rho m}{2}(f(t)-kv(t)) + \frac{\rho J}{2l}(k\omega(t)-\tau(t)) \end{aligned} \tag{2}$$

where k is a positive constant. Then, (1) becomes

$$\begin{bmatrix} \dot{x}(t) \\ \dot{y}(t) \\ \dot{\phi}(t) \\ \dot{v}(t) \\ \dot{\omega}(t) \end{bmatrix} = \begin{bmatrix} v(t)\cos\phi(t) \\ v(t)\sin\phi(t) \\ \omega(t) \\ f(t)-kv(t) \\ \tau(t)-k\omega(t) \end{bmatrix} \tag{3}$$

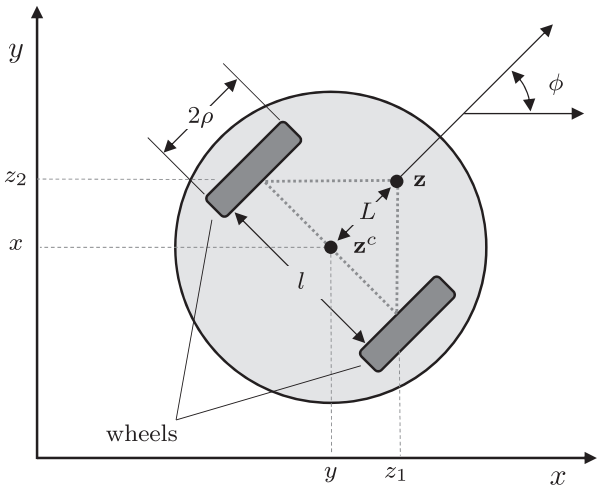

Fig. 1. Nonholonomic differential two-wheels drive vehicle.

where $f(t)$ and $\tau(t)$ denote the new control force and torque inputs. To avoid the saturation of the control torques, the new control inputs must be computed such that $|f(t)| \leq F$ and $|\tau(t)| \leq T\ \forall t$, where F and T are two positive constants to be determined based on the maximum admissible linear and angular velocities.

Lemma 2.1. *Consider the kinematics and dynamics model in equation (3). If* $|v(0)| \leq F/k$ *and* $|\omega(0)| \leq T/k$, *then* $|v(t)| \leq F/k$ *and* $|\omega(t)| \leq T/k\ \forall t \geq 0$.

Proof. First, let us prove that v remains bounded. To this end, let us consider the following Lyapunov-candidate function[2]

$$V_v = \frac{v^2}{2}$$

Taking its time-derivative we obtain

$$\dot{V}_v = v(f-kv) \leq |v|(F-k|v|)$$

which yields that $\dot{V}_v < 0$ whenever $|v(t)| > F/k$. Therefore, since $|v(0)| \leq F/k$ and V_v is decreasing for $|v(t)| > F/k$, we can conclude that $|v(t)| \leq F/k\ \forall t \geq 0$.

Now, let us consider ω. Letting $V_\omega = \omega^2/2$ and taking its time-derivative yields

$$\dot{V}_\omega = \omega(\tau - k\omega) \leq |\omega|(T-k|\omega|)$$

which is negative for any $|\omega(t)| > T/k$. Therefore, following similar arguments used in the case of the linear velocity, we can conclude that $|\omega(t)| \leq T/k\ \forall t \geq 0$. □

Having found suitable bounds for the linear and angular velocities, we can now compute F and T. First, note that in order to avoid exceeding the saturation constraint on the control torques, the new control inputs must satisfy

$$|f(t)-kv(t)| \leq \frac{M}{m\rho}$$

$$|\tau(t)-k\omega(t)| \leq \frac{lM}{J\rho}$$

Therefore, by choosing $F = \frac{M}{2m\rho}$ and $T = \frac{lM}{2J\rho}$ and assuming that $|v(0)| \leq F/k$ and $|\omega(0)| \leq T/k$, we can verify that the above inequality constraints are satisfied $\forall t \geq 0$.

2.2. Input–output linearization

The design of control laws to regulate and stabilize the motion of a nonholonomic system can be challenging. For instance, Brockett's celebrated theorem (1983) yields that nonholonomic systems, including (3), cannot be asymptotically stabilized by the application of smooth pure state feedback. Moreover, the considered kinematics and dynamics model (3) cannot be input-state linearized (Sarkar et al., 1994; Yamamoto and Yun, 1994). Notwithstanding, it has been shown that a nonholonomic system, such as (3), can be input–output feedback linearized if an appropriate pair of output equations are selected (Sarkar et al., 1994; Yamamoto and Yun, 1994; Lawton et al., 2003). Herein, we closely follow the output feedback linearization performed in the latter efforts by choosing the new output equations to be the coordinates of a reference point, namely $\mathbf{z}$, located in front of the vehicle and given by

$$\mathbf{z} = \begin{bmatrix} z_1 \\ z_2 \end{bmatrix} = \begin{bmatrix} x + L\cos\phi \\ y + L\sin\phi \end{bmatrix} \tag{4}$$

where L is a positive constant (see Figure 1). Now, by taking the first and second time-derivative of (4) and designing the control inputs f and τ as

$$\begin{bmatrix} f \\ \tau \end{bmatrix} = \begin{bmatrix} \cos\phi & \sin\phi \\ -\dfrac{\sin\phi}{L} & \dfrac{\cos\phi}{L} \end{bmatrix} \begin{bmatrix} u_1 + v\omega\sin\phi + L\omega^2\cos\phi \\ u_2 - v\omega\cos\phi + L\omega^2\sin\phi \end{bmatrix} \tag{5}$$

we can show that (3) is input–output linearized as

$$\ddot{\mathbf{z}} = \mathbf{u} - k\dot{\mathbf{z}} \tag{6}$$

where $\mathbf{u} = [u_1, u_2]^{\mathrm{T}}$ is the control input for the input–output linearized model. The complete input–output feedback transformation of (3) with state vector $[z_1, z_2, \dot{z}_1, \dot{z}_2, \phi]^{\mathrm{T}}$ can be written in the following form:

$$\begin{bmatrix} \dot{z}_1 \\ \dot{z}_2 \\ \ddot{z}_1 \\ \ddot{z}_2 \end{bmatrix} = \begin{bmatrix} 0 & 0 & 1 & 0 \\ 0 & 0 & 0 & 1 \\ 0 & 0 & -k & 0 \\ 0 & 0 & 0 & -k \end{bmatrix} \begin{bmatrix} z_1 \\ z_2 \\ \dot{z}_1 \\ \dot{z}_2 \end{bmatrix} + \begin{bmatrix} 0 & 0 \\ 0 & 0 \\ 1 & 0 \\ 0 & 1 \end{bmatrix} \begin{bmatrix} u_1 \\ u_2 \end{bmatrix} \tag{7}$$

$$\dot{\phi} = -\frac{\dot{z}_1\sin\phi}{L} + \frac{\dot{z}_2\cos\phi}{L} \tag{8}$$

where the last equation represents the internal dynamics. In contrast to the input–output feedback linearized structure (7), which is controllable, the internal dynamics (8) are unobservable and uncontrollable. However, we can show that (8) is at least stable by assessing its zero dynamics, that is, when $z_1 = z_2 = \dot{z}_1 = \dot{z}_2 = 0$. Clearly, if $\dot{z}_1 = \dot{z}_2 = 0$, then $\dot{\phi} = 0$, which implies that the internal dynamics are Lagrange stable.

Remark 2.1. *The control input for the linearized model* $\mathbf{u}_i$ *must still comply with the saturation constraint experienced by the wheels' control torques. Assuming that the initial conditions of the systems satisfy* $|v(0)| \leq F/k$ *and* $|\omega(0)| \leq T/k$, *such that* $|v(t)| \leq F/k$ *and* $|\omega(t)| \leq T/k$ *for all* $t \geq 0$ *(see Lemma 2.1), it can be shown that* $\sup_{t\geq 0}|\tau_L(t)| = \sup_{t\geq 0}|\tau_R(t)| \leq M$ *if*

$$k^2 \geq \max\left\{LT^2F^{-1}, FL^{-1}\right\}$$
$$\|\mathbf{u}(t)\| \leq \bar{\mu} = \min\left\{F - \frac{LT^2}{k^2}, LT - \frac{TF}{k^2}\right\}, \quad \forall\, t \geq 0$$

Moreover, we have that if we choose $L = F/T$, *then, the limit on the admissible control input (i.e.* $\bar{\mu}$*) attains its maximum with* $\bar{\mu} = F(1 - Tk^{-2})$ *and* $k > \sqrt{T}$.

Lemma 2.2. *Consider the linear model in (6) and let* $\eta = \bar{\mu}/k$. *Assume that* $\|\dot{\mathbf{z}}(0)\| \leq \eta$. *Then,* $\|\dot{\mathbf{z}}(t)\| \leq \eta\ \forall\, t \geq 0$.

Proof. The proof is similar to that of Lemma 2.1 and uses $V_z = \dot{\mathbf{z}}^2/2$ as Lyapunov-candidate function. □

In the remaining part of the paper, we will use the linearized representation in (6), along with the control input $\mathbf{u}$, to address the dynamics of the system and achieve the control objectives.

2.3. Control objectives

Having linearized the mathematical model for the motion of the nonholonomic vehicle, we now state the main control objectives. First, we would like to design the control input $\mathbf{u}$ such that the motion of the vehicle converges to a desired trajectory characterized by the triplet $\{\mathbf{z}^d(t), \dot{\mathbf{z}}^d(t), \ddot{\mathbf{z}}^d(t)\}$, where $\mathbf{z}^d \in \Re^2$, $\dot{\mathbf{z}}^d \in \Re^2$, and $\ddot{\mathbf{z}}^d \in \Re^2$ represent the desired position, velocity, and acceleration, respectively. Second, we would like to enforce a safe distance between the vehicle and any obstacle (as well as any other vehicle) at all times despite uncertainties in the localization of obstacles. To this end, we will propose a twofold control law comprised of a trajectory tracking part and a collision avoidance input. Mathematically, we propose $\mathbf{u}$ to be given by

$$\mathbf{u}(t) = \mathbf{u}^o(t) + \mathbf{u}^a(t) \tag{9}$$

where $\mathbf{u}^o \in \Re^2$ and $\mathbf{u}^a \in \Re^2$ are the trajectory tracking and collision avoidance control laws, respectively. The trajectory tracking control will be designed such that the error between the position of the vehicle and its desired trajectory, denoted as $\tilde{\mathbf{z}}(t) = \mathbf{z}(t) - \mathbf{z}^d(t)$, converges to zero. The avoidance control law will be designed such that vehicle maintains a safe distance from any other agent at all times.

3. Bounded trajectory tracking control

In this section, we introduced the trajectory tracking control input $\mathbf{u}^o$ and show that the motion of the nonholonomic vehicle, described by the input–output linearized equation

in (6), converges to the desired trajectory $\mathbf{z}^d(t)$. Accordingly, we propose the trajectory tracking control law to be computed as

$$\mathbf{u}^o(t) = \ddot{\mathbf{z}}^d(t) + k\dot{\mathbf{z}}^d(t) - \mathbf{g}(\tilde{\mathbf{z}}(t)) \tag{10}$$

where $\mathbf{g} : \Re^2 \to \Re^2$ is a continuous vector function satisfying the following properties.

P1. $\mathbf{g}(\mathbf{x}) = \mathbf{0}$ if and only if $\mathbf{x} = \mathbf{0}$.
P2. $\|\mathbf{g}(\mathbf{x})\| \leq G\ \forall \mathbf{x} \in \Re^2$ and some $G \in (0, \bar{\mu}]$.
P3. $\mathbf{g}$ is monotonically non-decreasing, i.e. $(\mathbf{g}(\mathbf{x}) - \mathbf{g}(\mathbf{y}))^{\mathrm{T}} (\mathbf{x} - \mathbf{y}) \geq 0\ \forall \mathbf{x}, \mathbf{y} \in \Re^2$.
P4. $\partial \mathbf{g}(\mathbf{x}) / \partial \mathbf{x}$ is piecewise continuous, symmetric, and bounded $\forall \mathbf{x} \in \Re^2$.

Remark 3.1. *Examples of continuous bounded vector functions satisfying the above properties include*

(a) $\mathbf{g}(\mathbf{x}) = \kappa \mathbf{x}$ *for* $\|\mathbf{x}\| \leq \frac{G}{\kappa}$, $\mathbf{g}(\mathbf{x}) = G\frac{\mathbf{x}}{\|\mathbf{x}\|}$ *otherwise, where* $\kappa > 0$;
(b) $\mathbf{g}(\mathbf{x}) = G\frac{\mathbf{x}^{2p-1}}{1 + \|\mathbf{x}\|^{2p-1}}$, *where p is a positive integer number*;
(c) $\mathbf{g}(\mathbf{x}) = 2G\pi^{-1}[\arctan(x_1), \arctan(x_2)]^{\mathrm{T}}$.

We now prove that (10) guarantees asymptotic tracking of a reference trajectory when the avoidance control vanishes, i.e. $\mathbf{u}^a \equiv \mathbf{0}$.

Theorem 3.1 (Convergence to desired trajectory)**.** *Consider the dynamical system in (6) with control input given by (9) and (10) for* $\mathbf{u}^a \equiv \mathbf{0}$ *and* $G \in (0, \bar{\mu}]$. *Assume that* $\|\ddot{\mathbf{z}}^d(t) + k\dot{\mathbf{z}}^d(t)\| \leq \bar{\mu} - G\ \forall t \geq 0$. *Then,* $\tilde{\mathbf{z}}(t)$, $\dot{\tilde{\mathbf{z}}}(t)$, *and* $\ddot{\tilde{\mathbf{z}}}(t)$ *converge to zero asymptotically.*

Proof. First, we will show that $\exists c_0 \in \Re$ such that $\int_C \mathbf{g}(\tilde{\mathbf{z}})\, d\tilde{\mathbf{z}} \geq c_0$, where $C \subset \Re^2$ denotes the path traveled by the vehicle from $\tilde{\mathbf{z}}(0)$ to $\tilde{\mathbf{z}}(t)$. Then, using this result, we will show that $\tilde{\mathbf{z}}(t)$, $\dot{\tilde{\mathbf{z}}}(t)$, and $\ddot{\tilde{\mathbf{z}}}(t)$ converge to zero asymptotically.

Consider a continuous vector function $\mathbf{g}$ satisfying properties P1 to P4. Since $\partial \mathbf{g}(\tilde{\mathbf{z}}) / \partial \tilde{\mathbf{z}}$ exists and is symmetric, we have that $\mathbf{g}$ is the gradient of some function $\mathcal{G} : \Re^2 \to \Re$, i.e. $\mathbf{g}(\tilde{\mathbf{z}}) = \partial \mathcal{G}(\tilde{\mathbf{z}}) / \partial \tilde{\mathbf{z}}$ (Rockafellar, 1966, 1968). Moreover, since $\mathbf{g}(\tilde{\mathbf{z}})$ is monotonically non-decreasing $\forall \tilde{\mathbf{z}} \in \Re^2$, we can conclude that $\mathcal{G}(\tilde{\mathbf{z}})$ is convex (Rockafellar, 1966), which in turns implies that $\mathcal{G}(\tilde{\mathbf{z}}) \geq \bar{c}_0$ for all $\tilde{\mathbf{z}} \in \Re^2$ and some $\bar{c}_0 \in \Re$. Therefore,

$$\int_C \mathbf{g}(\tilde{\mathbf{z}})\, d\tilde{\mathbf{z}} = \mathcal{G}(\tilde{\mathbf{z}}(t)) - \mathcal{G}(\tilde{\mathbf{z}}(0)) \geq c_0$$

where we have chosen $c_0 = \bar{c}_0 - \mathcal{G}(\tilde{\mathbf{z}}(0))$.

Now, assume that the vehicle's control input is given by (9) and (10), that $\mathbf{u}^a \equiv \mathbf{0}$, and let $\|\ddot{\mathbf{z}}^d(t) + k\dot{\mathbf{z}}^d(t)\| \leq \bar{\mu} - G$ (which implies that $\|\mathbf{u}(t)\| \leq \bar{\mu}$). Then, (6) can be rewritten in terms of the error dynamics as

$$\ddot{\tilde{\mathbf{z}}} = -k\dot{\tilde{\mathbf{z}}} - \mathbf{g}(\tilde{\mathbf{z}}) \tag{11}$$

Next, let us consider the following non-negative Lyapunov-candidate function

$$V_o(t) = \frac{1}{2}\dot{\tilde{\mathbf{z}}}^{\mathrm{T}}(t)\dot{\tilde{\mathbf{z}}}(t) + \int_C \mathbf{g}(\tilde{\mathbf{z}})\, d\tilde{\mathbf{z}} - c_0 = \frac{1}{2}\dot{\tilde{\mathbf{z}}}^{\mathrm{T}}(t)\dot{\tilde{\mathbf{z}}}(t) + \int_0^t \dot{\tilde{\mathbf{z}}}^{\mathrm{T}}(\sigma)\, \mathbf{g}(\tilde{\mathbf{z}}(\sigma))\, d\sigma - c_0$$

Taking its time-derivative and substituting by (11) yields

$$\dot{V}_o = \dot{\tilde{\mathbf{z}}}^{\mathrm{T}}\ddot{\tilde{\mathbf{z}}} + \dot{\tilde{\mathbf{z}}}^{\mathrm{T}}\mathbf{g}(\tilde{\mathbf{z}}) = -k\dot{\tilde{\mathbf{z}}}^{\mathrm{T}}\dot{\tilde{\mathbf{z}}} \leq 0 \tag{12}$$

Then, integrating both sides of (12) yields that $V_o(t) \leq V_o(0) \leq \infty$, which also implies that $\dot{\tilde{\mathbf{z}}} \in \mathcal{L}_\infty \cap \mathcal{L}_2$. Similarly, from (11) and P2, we have that $\ddot{\tilde{\mathbf{z}}} \in \mathcal{L}_\infty$. Applying Barbalat's Lemma (Khalil, 2002), we obtain that $\dot{\tilde{\mathbf{z}}} \to \mathbf{0}$. Now, returning to (11) and differentiating with respect to time yields

$$\dddot{\tilde{\mathbf{z}}} = -k\ddot{\tilde{\mathbf{z}}} - \frac{\partial \mathbf{g}^{\mathrm{T}}(\tilde{\mathbf{z}})}{\partial \tilde{\mathbf{z}}}\dot{\tilde{\mathbf{z}}}$$

from which we obtain that $\dddot{\tilde{\mathbf{z}}}$ is bounded. Then, since $\int_0^t \ddot{\tilde{\mathbf{z}}}(\sigma)\, d\sigma \to -\dot{\tilde{\mathbf{z}}}(0) < \infty$, we can once again invoke Barbalat's Lemma and obtain that $\ddot{\tilde{\mathbf{z}}} \to \mathbf{0}$. Finally, using (11) and the convergence results for $\ddot{\tilde{\mathbf{z}}}$ and $\dot{\tilde{\mathbf{z}}}$, we have that $\mathbf{g}(\tilde{\mathbf{z}}) \to \mathbf{0}$, which implies that $\tilde{\mathbf{z}} \to \mathbf{0}$ and the proof is complete. □

The above theorem establishes convergence of the vehicle to the desired trajectory in terms of the new system's state vector $\mathbf{z}$. Unfortunately, it does not provide information about the orientation of the vehicle.[3] From (8) and Theorem 3.1, we can only conclude that $\dot{\phi}$ remains bounded. However, we can prove that for the special case of set-point regulation, that is, when $\ddot{\mathbf{z}}^d(t) \equiv \dot{\mathbf{z}}^d(t) \equiv \mathbf{0}$, and for an appropriate choice of control function $\mathbf{g}$, $\dot{\phi}$ vanishes and ϕ stabilizes at a constant value.

Theorem 3.2 (Set-point stabilization)**.** *Consider the dynamical system in (6) with control input given by (9) and (10) for* $\mathbf{u}^a \equiv \mathbf{0}$. *Let* $\ddot{\mathbf{z}}^d(t) \equiv \dot{\mathbf{z}}^d(t) \equiv \mathbf{0}$ *and assume that* $\mathbf{g}(\tilde{\mathbf{z}})$ *satisfies properties P1 to P4 in addition to*

$$\mathbf{g}(\tilde{\mathbf{z}}) = \kappa\tilde{\mathbf{z}}, \qquad \text{for } \|\tilde{\mathbf{z}}\| \leq B_z$$

where $\kappa > 0$, $G \in (0, \bar{\mu}]$, *and* $0 < B_z \leq G/\kappa$. *Then, the following statements are true.*

(i) *The states* $\dot{\mathbf{z}}$, $\tilde{\mathbf{z}}$, *and* $\dot{\phi}$ *globally asymptotically vanish.*
(ii) *The states* $\dot{\mathbf{z}}$, $\tilde{\mathbf{z}}$, *and* $\dot{\phi}$ *locally exponentially vanish.*
(iii) *The state* ϕ *converges to a constant value.*

Proof. Statement (i) follows directly from Theorem 3.1. To prove the second claim, let us first assume that $\exists t_0 \geq 0$ such that $\|\tilde{\mathbf{z}}(t)\| \leq B_z\ \forall t \geq t_0$ (note that such t_0 exists since $\tilde{\mathbf{z}}(t) = 0$ is globally asymptotically stable). Then, consider the following Lyapunov-candidate function

$$V_s = \frac{1}{2}\dot{\mathbf{z}}^{\mathrm{T}}\dot{\mathbf{z}} + \kappa\tilde{\mathbf{z}}^{\mathrm{T}}\tilde{\mathbf{z}} + \frac{1}{2}(\dot{\mathbf{z}} + k\tilde{\mathbf{z}})^{\mathrm{T}}(\dot{\mathbf{z}} + k\tilde{\mathbf{z}}) \tag{13}$$

which is both lower and upper bounded as

$$\alpha_1 \left\| \begin{bmatrix} \dot{\mathbf{z}} \\ \tilde{\mathbf{z}} \end{bmatrix} \right\|^2 \leq V_s \leq \alpha_2 \left\| \begin{bmatrix} \dot{\mathbf{z}} \\ \tilde{\mathbf{z}} \end{bmatrix} \right\|^2$$

for $\alpha_2 = \max\{3/2, \kappa + k^2\} > \alpha_1 = \min\{1/2, \kappa\} > 0$. Taking the time derivative of (13) yields

$$\dot{V}_s = \dot{\mathbf{z}}^{\mathrm{T}}\ddot{\mathbf{z}} + 2\kappa_i\tilde{\mathbf{z}}^{\mathrm{T}}\dot{\mathbf{z}} + (\dot{\mathbf{z}} + k\tilde{\mathbf{z}})^{\mathrm{T}}(\ddot{\mathbf{z}} + k_i\dot{\mathbf{z}}) \qquad (14)$$

which for all $\dot{\mathbf{z}} \in \Re^2$ and $\|\tilde{\mathbf{z}}\| \leq B_z$ becomes

$$\begin{aligned}\dot{V}_s &= 2\dot{\mathbf{z}}^{\mathrm{T}}(-k\dot{\mathbf{z}} - \kappa\tilde{\mathbf{z}}) + 2\kappa\tilde{\mathbf{z}}^{\mathrm{T}}\dot{\mathbf{z}} + k\dot{\mathbf{z}}^{\mathrm{T}}\dot{\mathbf{z}} \\ &\quad + \kappa\tilde{\mathbf{z}}^{\mathrm{T}}(-k\dot{\mathbf{z}} - \kappa\tilde{\mathbf{z}}) + \kappa k\tilde{\mathbf{z}}^{\mathrm{T}}\dot{\mathbf{z}} = -k\dot{\mathbf{z}}^{\mathrm{T}}\dot{\mathbf{z}} - \kappa^2\tilde{\mathbf{z}}^{\mathrm{T}}\tilde{\mathbf{z}} \\ &\leq -\alpha_3 \left\| \begin{bmatrix} \dot{\mathbf{z}} \\ \tilde{\mathbf{z}} \end{bmatrix} \right\|^2\end{aligned}$$

where $\alpha_3 = \min\{k, \kappa^2\}$. Therefore, we conclude that $\dot{\mathbf{z}}$ and $\tilde{\mathbf{z}}^{\mathrm{T}}$ converge locally exponentially to zero (Khalil, 2002), that is,

$$\left\| \begin{bmatrix} \dot{\mathbf{z}}(t) \\ \tilde{\mathbf{z}}(t) \end{bmatrix} \right\| \leq \sqrt{\frac{\alpha_2}{\alpha_1}} \left\| \begin{bmatrix} \dot{\mathbf{z}}(t_0) \\ \tilde{\mathbf{z}}(t_0) \end{bmatrix} \right\| e^{-\frac{\alpha_3}{2\alpha_2}(t-t_0)}$$

for all $\dot{\mathbf{z}}(t_0) \in \Re^2$ and $\|\tilde{\mathbf{z}}(t_0)\| \leq B_z$. Similarly, from (8), we have that

$$\begin{aligned}|\dot{\phi}(t)| &\leq \frac{1}{L} \left\| \begin{bmatrix} -\sin\phi(t) \\ \cos\phi(t) \end{bmatrix} \right\| \|\dot{\mathbf{z}}(t)\| \\ &\leq \frac{1}{L}\sqrt{\frac{\alpha_2}{\alpha_1}} \left\| \begin{bmatrix} \dot{\mathbf{z}}(t_0) \\ \tilde{\mathbf{z}}(t_0) \end{bmatrix} \right\| e^{-\frac{\alpha_3}{2\alpha_2}(t-t_0)} \qquad (15)\end{aligned}$$

which implies that $\dot{\phi} \to 0$ exponentially.

Now, let us prove the last statement. We will show that for any arbitrarily small $\varepsilon > 0$, $\exists T_0 < \infty$ such that

$$|\phi(t) - \phi(T_0)| < \varepsilon, \qquad \forall\, t > T_0$$

To this end, let us consider (15). Integrating both sides with respect to time from $T_0 \geq t_0$ to t yields

$$\left| \int_{T_0}^{t} \dot{\phi}(\sigma)\, d\sigma \right| \leq \int_{T_0}^{t} |\dot{\phi}(\sigma)|\, d\sigma = \frac{2\alpha_2}{L\alpha_3}\sqrt{\frac{\alpha_2}{\alpha_1}} \left\| \begin{bmatrix} \dot{\mathbf{z}}(t_0) \\ \tilde{\mathbf{z}}(t_0) \end{bmatrix} \right\| \left(e^{-\frac{\alpha_3}{2\alpha_2}(T_0 - t_0)} - e^{-\frac{\alpha_3}{2\alpha_2}(t-t_0)} \right)$$

Then, for any $\varepsilon > 0$ and

$$T_0 = t_0 + \max\left\{ 2\frac{\alpha_2}{\alpha_3} \ln\left(\frac{2\alpha_2}{\varepsilon L\alpha_3}\sqrt{\frac{\alpha_2}{\alpha_1}} \left\| \begin{bmatrix} \dot{\mathbf{z}}(t_0) \\ \tilde{\mathbf{z}}(t_0) \end{bmatrix} \right\| \right), 0 \right\}$$

we can show that $|\phi(t) - \phi(T_0)| < \varepsilon$, $\forall\, t > T_0$, which completes the proof. □

Up to now, we have assumed that the avoidance control is zero. In the next section, when we address the collision avoidance problem, we will design the avoidance control input such that it is zero when other obstacles and agents are sufficiently away from the vehicle. In that case, we can apply Theorems 3.1 and 3.2 whenever the vehicle is at a safe distance from other obstacles and guarantee convergence to the desired trajectory or set-point, respectively.

4. Collision avoidance control under sensing uncertainties

In the previous section, we introduced a bounded control law that guarantees convergence of an autonomous vehicle to a desired trajectory. Herein, we will develop a complementary avoidance control strategy to enforce collision-free trajectories. We will explicitly consider the interaction of two agents (either a pair of nonholonomic vehicles or a vehicle and an obstacle), named the *i*th vehicle and the *j*th agent.[4] To differentiate between agents' variables (e.g. position, velocity, and control gains), we will append the subscripts i and j to the notation already discussed (see Appendix A for a complete list of the notation).

Ideally, the avoidance control should guarantee a safe distance $r_{ij} > 0$ between the *i*th vehicle and any *j*th obstacle (or agent) at all times and should not interfere with the trajectory tracking control when the obstacles are safely away.

In order to design the avoidance control law, we first make the following assumptions about the obstacle's localization process.

Assumption 4.1. *The ith vehicle can obtain (or sense) the position of the jth agent, either via the use of on-board localization sensors (e.g. sonar radars, computer vision systems, and infrared lasers) or the broadcast of position information among agents, whenever the latter is within the bounded sensing range of the ith vehicle (denoted by $\mathcal{D}_{ij}$ in Figure 2).*

Remark 4.1. *In this paper, we assume that the ith vehicle senses the position of the jth agent's center, i.e. $\mathbf{z}_j^c$. Similar results will follow if the ith vehicle can detect or know the position of the point in front of the jth agent, i.e. $\mathbf{z}_j$.*

Assumption 4.2. *The localization process of the jth agent by the ith vehicle is subjected to sensing uncertainties (e.g. measurement errors due to delays, noises, quantization, and disconnections). Mathematically, we suppose that the ith vehicle can detect the jth obstacle as being located at $\hat{\mathbf{z}}_j(t) = \mathbf{z}_j^c + \mathbf{d}_{ij}(t)$, where $\mathbf{z}_j^c \in \Re^2$ are the true coordinates of the jth obstacle's geometric center and $\mathbf{d}_{ij} \in \Re^2$ is the uncertainty incurred in the localization process (e.g. detection errors due to delays, quantization, and noise). Moreover, the measurement error or sensing uncertainty is known to be bounded by some constant Δ_{ij}, i.e. $\|\mathbf{d}_{ij}(t)\| \leq \Delta_{ij}$ $\forall\, t \geq 0$. Geometrically, this implies that the obstacle's position estimate $\hat{\mathbf{z}}_j$ lies within the circular area of uncertainty with radius Δ_{ij} and centered at $\mathbf{z}_j^c$ (represented as $\hat{\mathcal{Z}}_j$ in Figure 2).*

4.1. Formulation of the collision avoidance problem

We address the collision avoidance problem similar to Leitmann and Skowronski (1977), where the concept of avoidance control was introduced. Leitmann and Skowronski

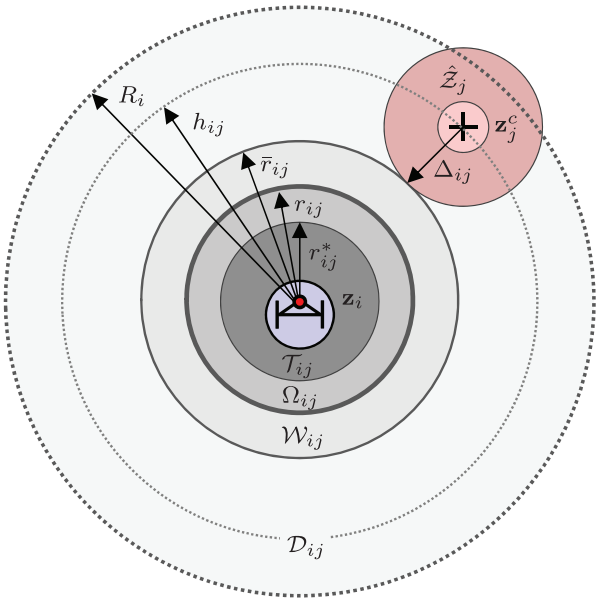

Fig. 2. Antitarget ($\mathcal{T}_{ij}$), avoidance (Ω_{ij}), conflict ($\mathcal{W}_{ij}$), and detection ($\mathcal{D}_{ij}$) regions for the *i*th vehicle. The circular area $\hat{\mathcal{Z}}_j$ represents the bounded region of uncertainty around the *j*th obstacle.

formulated sufficient conditions, based on Lyapunov-based analysis, that guarantee that the trajectories of a pair of agents, emanating from the outside of a given set, namely the *Avoidance Set*, do not enter the set at any given time. One of the main advantages of their control formulation is that the avoidance control does not need to be active at all times. Instead, the avoidance control takes effect once the agents enter a bounded set, namely the *Safety Set*, which encloses but does not include the Avoidance Set.

Inspired by Leitmann and Skowronski's concept of Avoidance and Safety Sets, we now introduce the following definitions.

We define an *Antitarget region* (see Figure 2), $\mathcal{T}_{ij} \subset \Re^4$, as the collision zone for the *i*th and *j*th agents, i.e.

$$\mathcal{T}_{ij} = \left\{ \mathbf{Z} : \mathbf{Z} \in \Re^4, \left\| \mathbf{z}_i - \mathbf{z}^c_j \right\| \leq r^*_{ij} \right\}$$

where $\mathbf{Z} = [\mathbf{z}_i^{\mathrm{T}}, \mathbf{z}_j^{c\mathrm{T}}]^{\mathrm{T}}$ and r^*_{ij} denotes the minimum safe separation distance between both agents. Similarly, we define an *Avoidance region*, $\Omega_{ij} \supseteq \mathcal{T}_{ij}$, as the zone in which the two agents are not allowed to enter at any given time. Mathematically,

$$\Omega_{ij} = \left\{ \mathbf{Z} : \mathbf{Z} \in \Re^4, \left\| \mathbf{z}_i - \mathbf{z}^c_j \right\| \leq r_{ij} \right\}$$

where $r_{ij} \geq r^*_{ij}$ is the desired minimum separation between both agents.[5] Note that, if we design a control policy such that $\mathbf{z}_i$ and $\mathbf{z}^c_j$ avoid Ω_{ij}, then we have that they must also avoid $\mathcal{T}_{ij}$.

Now, consider the acceleration and control input constraints on the *i*th vehicle. Since its acceleration components are bounded, a control policy aimed to avoid Ω_{ij} needs to be implemented with enough anticipation, such that the *i*th vehicle has sufficient time to decelerate and prevent a collision. Consequently, we define a *Conflict region*, $\mathcal{W}_{ij} \subset \Re^4$, as

$$\mathcal{W}_{ij} = \left\{ \mathbf{Z} : \mathbf{Z} \in \Re^4, r_{ij} < \left\| \mathbf{z}_i - \mathbf{z}^c_j \right\| \leq \bar{r}_{ij} \right\}$$

where $\bar{r}_{ij} > r_{ij}$ is a lower bound on the distance that the *i*th vehicle can come from the other agent and still be able to decelerate and avoid Ω_{ij}. Thus any collision avoidance strategy for the *i*th vehicle must take effect as soon as $\mathbf{z}_i$ and $\mathbf{z}^c_j$ enter $\mathcal{W}_{ij}$.

Finally, in order for the problem to be well-defined, it is assumed that $\mathcal{W}_{ij}$ lies within the *Detection region*, $\mathcal{D}_{ij} \subseteq \Re^4$, of the *i*th agent, defined as

$$\mathcal{D}_{ij} = \left\{ \mathbf{Z} : \mathbf{Z} \in \Re^4, \left\| \mathbf{z}_i - \mathbf{z}^c_j \right\| \leq R_i \right\}$$

where $R_i > \bar{r}_{ij}$ is the detection radius. That is, the *i*th agent can detect any obstacle or agent inside the Detection region.

According to the above definitions, we can state the control objective as follows. Given Δ_{ij}, r^*_{ij}, and R_i, design control input $\mathbf{u}^a_i(t)$ and Avoidance and Conflict radii r_{ij} and $\bar{r}_{ij}$ such that $[\mathbf{z}_i^{\mathrm{T}}(t), \mathbf{z}_j^{c\mathrm{T}}(t)]^{\mathrm{T}} \notin \Omega_{ij}$ for all $t \geq 0$, where $\Omega_{ij} \supseteq \mathcal{T}_{ij}$.

4.2. Bounded avoidance control

In order to guarantee collision avoidance between the *i*th and *j*th agents, we propose the use of the following control law

$$\mathbf{u}^a_i(t) = -\frac{1}{\bar{\mu}_i} \left\| \frac{\partial V^a_{ij}(\mathbf{z}_i(t), \hat{\mathbf{z}}^c_j(t))}{\partial \mathbf{z}_i} \right\| \mathbf{u}^o_i(t) - \frac{\partial V^a_{ij}(\mathbf{z}_i(t), \hat{\mathbf{z}}^c_j(t))}{\partial \mathbf{z}_i} \tag{16}$$

where $V^a_{ij} : \Re^2 \to \Re$, termed the avoidance function, is given by

$$V^a_{ij} = \begin{cases} \Gamma_{ij} \left(\min \left\{ 0, \dfrac{\left\| \hat{\mathbf{z}}_{ij} \right\|^2 - R_i^2}{\left\| \hat{\mathbf{z}}_{ij} \right\|^2 - r_{ij}^2} \right\} \right)^2, & \text{if } \left\| \hat{\mathbf{z}}_{ij} \right\| \geq h_{ij} \\ -\bar{\mu}_i \left\| \hat{\mathbf{z}}_{ij} \right\| + c_{ij}, & \text{otherwise} \end{cases} \tag{17}$$

for $\hat{\mathbf{z}}_{ij} = \mathbf{z}_i - \hat{\mathbf{z}}^c_j$, $h_{ij} = \bar{r}_{ij} + \Delta_{ij}$, and

$$\Gamma_{ij} = \frac{\bar{\mu}_i \left(h_{ij}^2 - r_{ij}^2 \right)^3}{4 h_{ij} (R_i^2 - h_{ij}^2)(R_i^2 - r_{ij}^2)},$$

$$c_{ij} = \Gamma_{ij} \frac{(h_{ij}^2 - R_i^2)^2}{(h_{ij}^2 - r_{ij}^2)^2} + \bar{\mu}_i h_{ij}$$

The reader can easily verify that V_{ij}^a is nonnegative, almost everywhere continuously differentiable with

$$\frac{\partial V_{ij}^a}{\partial \mathbf{z}_i} = \begin{cases} \mathbf{0}, & \text{if } \left\|\hat{\mathbf{z}}_{ij}\right\| \geq R_i \\ \dfrac{K_{ij}^a(R_i^2 - \left\|\hat{\mathbf{z}}_{ij}\right\|^2)}{(\left\|\hat{\mathbf{z}}_{ij}\right\|^2 - r_{ij}^2)^3}\hat{\mathbf{z}}_{ij}, & \text{if } h_{ij} \leq \left\|\hat{\mathbf{z}}_{ij}\right\| < R_i \\ \bar{\mu}_i \dfrac{\hat{\mathbf{z}}_{ij}}{\left\|\hat{\mathbf{z}}_{ij}\right\|}, & \text{if } 0 < \left\|\hat{\mathbf{z}}_{ij}\right\| < h_{ij} \\ \text{not defined}, & \text{if } \left\|\hat{\mathbf{z}}_{ij}\right\| = 0 \end{cases} \tag{18}$$

where $K_{ij}^a = 4\Gamma_{ij}(R_i^2 - r_{ij}^2)$. Note that in contrast to the unboundedness of the avoidance functions and control inputs in Stipanović et al. (2007) and Mastellone et al. (2008), V_{ij}^a and $\mathbf{u}_i^a$ (proposed in this section) are bounded by c_{ij} and $\bar{\mu}_i$, respectively. In addition, it is worth to mention that the choice of avoidance function is not unique. Other almost everywhere continuously differentiable functions could be utilized in place of (17) if their gradients $\partial V_{ij}^a/\partial \mathbf{z}_i$ are $\mathbf{0}$ for $\left\|\hat{\mathbf{z}}_{ij}\right\| \geq R_i$ and $\bar{\mu}_i \frac{\hat{\mathbf{z}}_{ij}}{\left\|\hat{\mathbf{z}}_{ij}\right\|}$ for $0 < \left\|\hat{\mathbf{z}}_{ij}\right\| < h_{ij}$ (for an example, see Rodríguez-Seda et al., 2011b). We opted for (17) to resemble the avoidance functions proposed in Stipanović et al. (2007). Also note that the purpose of the first term in (16) is to attenuate or even turn off the tracking control when there is a high risk of a collision (when the agents enter the Conflict region). In general, maintaining the safety of the vehicle should be a priority over tracking a desired trajectory.

4.3. Collision avoidance under sensor uncertainties

We now prove that the avoidance control in (16) and (18) guarantees that the trajectories of the *i*th and *j*th agents do not intercept the Avoidance region. We first prove the statement for the noncooperative case, that is, when only the *i*th nonholonomic vehicle implements the avoidance control. Then, we address the case of cooperative avoidance, where both agents try to avoid each other.

Lemma 4.1. *(Rodríguez-Seda et al., 2011a) Consider a pair of two dynamical systems, namely the ith and jth vehicles. Let the ith nonholonomic vehicle, with input–output linearized equations of motion described by (6), have control inputs given as in (9) and (16). Assume that* $\exists\, \eta_j^c \geq 0$ *such that* $\left\|\dot{\mathbf{z}}_j^c(t)\right\| \leq \eta_j^c\ \forall t \geq 0$ *and define*

$$\beta_{ij}(t) = (\mathbf{z}_i(t) - \mathbf{z}_j^c(t))^{\mathrm{T}}\, \dot{\mathbf{z}}_i(t)$$

Choose $\theta_i \in \left(0, \sin^{-1}\left(\sqrt{r_\epsilon^2 - \Delta_{ij}^2}/r_\epsilon\right)\right)$ *and* $k_i \in (0, \bar{\mu}_i/\eta_j^c)$ *and define* $\delta_i = \theta_i r_\epsilon/(\eta_i + \eta_j^c)$, *where* $r_\epsilon \in (r_{ij}, \bar{r}_{ij}]$ *and* $r_{ij} > \Delta_{ij}$. *Suppose that for some* $t_0 \in [0, t_f - \delta_i]$ *we have that* $\|\dot{\mathbf{z}}_i(t_0)\| \leq \eta_i = \bar{\mu}_i/k_i$, $\left\|\mathbf{d}_{ij}(t)\right\| \leq \Delta_{ij}$, *and* $\left\|\mathbf{z}_i(t) - \mathbf{z}_j(t)\right\| \in [r_\epsilon, \bar{r}_{ij}]\ \forall\ t \in [t_0, t_f]$. *Then, we have that* $\beta_{ij}(t_f)$ *is lower bounded by*

$$\beta_{ij}(t_f) \geq \left\|\mathbf{z}_i(t_f) - \mathbf{z}_j(t_f)\right\| \left[-e^{-k_i\delta_i}\eta_i + \frac{\bar{\mu}_i}{r_\epsilon(k_i^2 + \omega_{ij}^2)}\left(k_i\sqrt{r_\epsilon^2 - \Delta_{ij}^2} + \omega_{ij}\Delta_{ij} - e^{-k_i\delta_i}\left(k_i\sqrt{r_\epsilon^2 - \Delta_{ij}^2}\cos\theta_i - k_i\Delta_{ij}\sin\theta_i + \omega_{ij}\sqrt{r_\epsilon^2 - \Delta_{ij}^2}\sin\theta_i + \omega_{ij}\Delta_{ij}\cos\theta_i\right)\right)\right] \tag{19}$$

where $\omega_{ij} = -(\eta_i + \eta_j^c)/r_\epsilon$.

Proof. See Appendix B. □

Remark 4.2. *Lemma 4.1 establishes the direction of motion of the ith vehicle with respect to the other agent. Mathematically, we have that* $\beta_{ij}(t)/\left\|\mathbf{z}_i(t) - \mathbf{z}_j^c(t)\right\|$ *is the scalar projection of the velocity vector* $\dot{\mathbf{z}}_i$ *onto the collision threat vector* $\mathbf{z}_i - \mathbf{z}_j^c$. *Thus,* $\beta_{ij}(t)$ *provides an indication of the direction of the ith vehicle's velocity vector with respect to the collision threat. For instance, if for some time* t_f, $\beta_{ij}(t_f) > 0$, *then we can conclude that at time* t_f *the ith vehicle is moving away from the jth agent.*

Theorem 4.1 (Noncooperative collision avoidance with uncertainties)**.** *Consider the ith nonholonomic system with input–output linearized equations of motion described by (6) and control input given by (9) and (16). Let* $k_i = \bar{\mu}_i/\eta_i > 0$ *and assume that* $[\mathbf{z}_i^{\mathrm{T}}(0), \mathbf{z}_j^{c\mathrm{T}}(0)]^{\mathrm{T}} \notin \mathcal{W}_{ij} \cup \Omega_{ij}$, $\|\dot{\mathbf{z}}_i(0)\| \leq \eta_i$, $\left\|\mathbf{d}_{ij}(t)\right\| \leq \Delta_{ij}$, *and* $\left\|\mathbf{z}_j^c(t)\right\| \leq \eta_j^c\ \forall t \geq 0$ *and some* $\eta_j^c \geq 0$. *Moreover, suppose there exist constants* $\eta_i > \eta_j^c$, $r_{ij} \geq r_{ij}^*$, $\epsilon > 0$, *and* $\theta_i \in \left(0, \sin^{-1}\left(\frac{\sqrt{r_\epsilon^2 - \Delta_{ij}^2}}{r_\epsilon}\right)\right)$ *such that*

$$\bar{r}_{ij} = (\theta_i + 1)(r_{ij} + \epsilon) < R_i - \Delta_{ij} \tag{20}$$

and

$$\left(k_i + \frac{\omega_{ij}\Delta_{ij}}{\sqrt{r_\epsilon^2 - \Delta_{ij}^2}}\right)\left(e^{k_i\delta_i} - \cos\theta_i\right) - \left(\omega_{ij} - \frac{k_i\Delta_{ij}}{\sqrt{r_\epsilon^2 - \Delta_{ij}^2}}\right)\sin\theta_i - \frac{r_\epsilon(k_i^2 + \omega_{ij}^2)}{k_i\sqrt{r_\epsilon^2 - \Delta_{ij}^2}}\sigma_{ij} \geq 0 \tag{21}$$

hold for $\sigma_{ij} = 1 + \frac{\eta_j^c}{\eta_i}e^{k_i\delta_i}$. *Then,* $[\mathbf{z}_i^{\mathrm{T}}(t), \mathbf{z}_j^{c\mathrm{T}}(t)]^{\mathrm{T}} \notin \Omega_{ij}$ $\forall t \geq 0$.

Proof. Consider the system in (6). Let the control input for the *i*th vehicle be given by (9) and (16). Assume that the *j*th agent's velocity is bounded by some $\eta_j^c \geq 0$ and that (20) and (21) hold. Let $k_i = \bar{\mu}_i/\eta_i$ where $\eta_i > \eta_j^c$ and assume that $\|\dot{\mathbf{z}}_i(0)\| \leq \eta_i$. Applying Lemma 2.2 we have that $\|\dot{\mathbf{z}}_i(t)\| \leq \eta_i\ \forall t \geq 0$.

Now, let us consider the following Lyapunov candidate function

$$V(t) = \frac{1}{4(\left\| \mathbf{z}_i(t) - \mathbf{z}_j^c(t) \right\|^2 - r_{ij}^2)^2}$$

Taking its time derivative yields

$$\begin{aligned}\dot{V}(t) &= \frac{(\mathbf{z}_i(t) - \mathbf{z}_j^c(t))^{\mathrm{T}} \dot{\mathbf{z}}_j^c(t) - \beta_{ij}(t)}{(\left\| \mathbf{z}_i(t) - \mathbf{z}_j^c(t) \right\|^2 - r_{ij}^2)^3} \\ &\leq \frac{\left\| \mathbf{z}_i(t) - \mathbf{z}_j^c(t) \right\| \eta_j^c - \beta_{ij}(t)}{(\left\| \mathbf{z}_i(t) - \mathbf{z}_j^c(t) \right\|^2 - r_{ij}^2)^3} \end{aligned} \quad (22)$$

Let $[\mathbf{z}_i^{\mathrm{T}}(0), \mathbf{z}_j^{c\mathrm{T}}(0)]^{\mathrm{T}} \notin \mathcal{W}_{ij} \cup \Omega$ and suppose that for some time $t > 0$, $\left\| \mathbf{z}_i(t) - \mathbf{z}_j^c(t) \right\| \to r_\epsilon = r_{ij} + \epsilon$ from above. Since $\left\| \mathbf{z}_i(0) - \mathbf{z}_j^c(0) \right\| > \bar{r}_{ij}$ and the velocities of the agents are bounded, it will take the agents some time Δt to reduce their distance from $\bar{r}_{ij}$ to r_ϵ. Therefore, we have that $[\mathbf{z}_i^{\mathrm{T}}(\tau), \mathbf{z}_j^{c\mathrm{T}}(\tau)]^{\mathrm{T}} \in \mathcal{W}_{ij}\ \forall \tau \in [t - \Delta t, t]$, where it is easy to demonstrate that $\Delta t \geq \delta_i = \frac{\bar{r}_{ij} - r_\epsilon}{\eta_i + \eta_j^c} = \frac{\theta_i r_\epsilon}{\eta_i + \eta_j^c}$. Then, applying Lemma 4.1 and using (20) and (21), it is easy to show that $\beta_{ij}(t) \geq \left\| \mathbf{z}_i(t) - \mathbf{z}_j^c(t) \right\| \eta_j$. Returning to (22), we finally obtain that $\dot{V}(t) \leq 0$ for $\left\| \mathbf{z}_i(t) - \mathbf{z}_j^c(t) \right\| \leq r_\epsilon$. The fact that $\mathbf{z}_i(t) - \mathbf{z}_j^c(t)$ is continuous and $\dot{V}(t)$ is nonpositive for $\left\| \mathbf{z}_i(t) - \mathbf{z}_j^c(t) \right\| \leq r_\epsilon$ implies that $V(t) < \infty$ (i.e. $V(t)$ is finite for any $t \geq 0$). Hence, the distance between $\mathbf{z}_i(t)$ and $\mathbf{z}_j^c(t)$ is uniformly ultimately lower bounded by r_ϵ, which further implies that $[\mathbf{z}_i^{\mathrm{T}}(t), \mathbf{z}_j^{c\mathrm{T}}(t)]^{\mathrm{T}} \notin \Omega_{ij}$ for all $t \geq 0$. □

The above theorem guarantees collision-free trajectories for the *i*th vehicle assuming the worst case scenario, i.e. when the *j*th agent does not apply any avoidance policy. In the following result, we present sufficient conditions for collision avoidance in a cooperative case where both agents implement the avoidance control. As it will be shown, the cooperative case relaxes the conservatism incurred in the noncooperative case, since the responsibility of avoidance is invested in both vehicles.

For simplicity, we assume that the Avoidance regions for both vehicles, termed in the following theorem as the first and second vehicles, are the same, i.e. $\Omega_{12} = \Omega_{21} = \Omega$. By definition, the respective Antitarget regions are also the same, i.e. $\mathcal{T}_{12} = \mathcal{T}_{21}$, whereas the Conflict and Detection regions do not need to be equal.

Theorem 4.2 (Cooperative collision avoidance with uncertainties)**.** *Consider a pair of vehicles, namely the first and second agents, with input–output linearized equations of motion described by (6) and control inputs given by (9) and (18) for $i \in \{1,2\}, i \neq j$. Let $k_i = \bar{\mu}_i / \eta_i$ and suppose that $\|\dot{\mathbf{z}}_i(0)\| \leq \eta_i$, $\left\| \mathbf{d}_{ij}(t) \right\| \leq \Delta_{ij}$, and $[\mathbf{z}_i(0), \mathbf{z}_j(0)] \notin \mathcal{W}_{ij} \cup \mathcal{W}_{ji} \cup \Omega$ for all $i,j \in \{1,2\}$, $i \neq j$. Furthermore, assume $\exists\ \epsilon > 0$, $\eta_i > 0$, $r_{ij} = r_{ji} \geq r_{ij}^* = r_{ji}^*$, and $\theta_i \in \left(0, \sin^{-1}\left(\frac{\sqrt{r_\epsilon^2 - \Delta_i^2}}{r_\epsilon}\right)\right)$ for $r_\epsilon = r_{ij} + \epsilon$ such that (20) and (21) hold for $\sigma_{ij} = 1 + L_j e^{k_i \delta_i} / r_\epsilon$ and $\forall\ i,j \in \{1,2\}, i \neq j$. Then, $[\mathbf{z}_1^{\mathrm{T}}(t), \mathbf{z}_2^{\mathrm{T}}(t)]^{\mathrm{T}} \notin \Omega\ \forall t \geq 0$.*

Proof. The proof follows similar to that of Theorem 4.1. See Rodríguez-Seda et al. (2011a) for further details. □

Remark 4.3. *If the collision avoidance control (18) is formulated in terms of $\mathbf{z}_j$ instead of $\mathbf{z}_j^c$, then Theorem 4.2 is equivalent to Theorem 4.1 in Rodríguez-Seda et al. (2011a).*

Theorems 4.1 and 4.2 guarantee collision avoidance between a pair of agents given the existence of constants η_i, r_{ij}, and θ_i satisfying (20) and (21). Theorem C.1 in Appendix C shows that a solution to the avoidance control problem, that is, the existence of such constants, always exists if the Detection radii of the *i*th and *j*th agents are large enough.

Remark 4.4. *From Theorem 3.1 we have that, once the ith agent is safely away from any other agent (i.e. when there is no other agent within the ith vehicle's Detection region, which implies that $\mathbf{u}_i^a \equiv \mathbf{0}$), the ith vehicle will converge to its desired trajectory. However, in general, we cannot guarantee that $\mathbf{u}_i^a \to \mathbf{0}$. In fact, there might be cases where symmetries in the vehicles' trajectories and Avoidance regions can lead to deadlocks or unwanted local minima, a fundamental problem of most potential (or avoidance) field function based navigation methods (Khatib, 1986; Koren and Borenstein, 1991). In this scenario, the tracking and avoidance control do not converge to zero (Rodríguez-Seda and Stipanović, 2013). Despite this problem, we will show by simulation and experimental examples that the uncertainties in the sensing process are enough to break the deadlocks. Especially, experiment 3 will force the vehicles to converge to opposite sides of the squared workspace, passing near the center of the workspace. This represents a symmetric case that maximizes the possibility of a deadlock or, even worse, a collision.*

5. Boundedness of control torques

The main contribution of this paper is the development of trajectory tracking with a collision avoidance control law that takes into consideration the vehicle dynamic and kinematic constraints as well as errors incurred during the localization of nearby obstacles. In Sections 2 through 4, we took careful consideration of the construction of the control inputs in order to guarantee that the proposed control law would not exceed the saturation limits of the wheels' admissible torques. In this section, we will explicitly demonstrate the boundedness of the control torques. To simplify the notation and follow the discussion of Sections 2 and 3, we will omit the subscripts *i* and *j*.

Theorem 5.1. *Consider the nonholonomic vehicle in (1). Assume that* $|v(0)| \leq F/k$ *and* $|\omega(0)| \leq T/k$. *Let the control input for the vehicle be given as in (2), (5), (9), (10), and (16) and define control parameters* $\bar{\mu} = F(1 - Tk^2)$ *and* $L = F/T$ *for* $F = M/2m\rho$, $T = lM/2J\rho$, *and* $k \geq \sqrt{T}$. *Then,* $|\tau_R(t)| \leq M$ *and* $|\tau_L(t)| \leq M \; \forall \, t \geq 0$.

Proof. First, note that the input of the linearized system is bounded by $\|\mathbf{u}\| \leq \|\mathbf{u}^o\| \left(1 - \frac{1}{\bar{\mu}} \left\| \frac{\partial V^a}{\partial \mathbf{z}} \right\| \right) + \left\| \frac{\partial V^a}{\partial \mathbf{z}} \right\| \leq \bar{\mu} \left(1 - \frac{1}{\bar{\mu}} \left\| \frac{\partial V^a}{\partial \mathbf{z}} \right\| \right) + \left\| \frac{\partial V^a}{\partial \mathbf{z}} \right\| = \bar{\mu}$. Then, consider the input–output feedback linearization law (5), which yields that

$$f = u_1 \cos\phi + u_2 \sin\phi + L\omega^2,$$
$$L\tau = -u_1 \sin\phi + u_2 \cos\phi - v\omega$$

Evaluating the maximum magnitude of f and τ yields that $|f| \leq \bar{\mu} + LT^2k^{-2} = F$ and $|\tau| \leq L^{-1}(\bar{\mu} + FTk^{-2}) = T$, where we used Lemma 2.1 to conclude that $|v| \leq F/k$ and $|\omega| \leq T/k$. Now, consider the control torques (2) applied at the wheels. Taking the maximum magnitude, we obtain that

$$|\tau_\star| \leq \frac{\rho m}{2}|f - kv| + \frac{\rho J}{2l}|\tau - k\omega| \leq \frac{\rho m}{2}(2F) + \frac{\rho J}{2l}(2T) = M, \qquad \text{for } \star \in R, L$$

Therefore, we can conclude that the control torques are bounded by M. □

6. Simulations

We now present two simulation examples that will illustrate the robustness and effectiveness of the proposed trajectory tracking with the collision avoidance control law. In the first example, we simulate the interaction of a single nonholonomic vehicle, moving in a circular path, with two static obstacles. In the second example, we simulate the cooperative behavior of two nonholonomic vehicles tracking an infinity-symbol shaped trajectory while avoiding collisions. Both simulation examples show the success of the tracking and avoidance control laws.

6.1. Example 1: One vehicle with static obstacles

We consider a nonholonomic autonomous vehicle with dynamics given by (1) and with inertial and physical parameters listed in Table 1. The control objective of the vehicle is to follow a circular trajectory (illustrated by the blue path in Figure 3) that evolves according to

$$\mathbf{z}_1^d(t) = \left[1.5\cos\left(\frac{\pi}{45}t\right) \text{ m}, 1.5\sin\left(\frac{\pi}{45}t\right) \text{ m}\right]^{\mathrm{T}}$$

Table 1. List of parameters for the simulation examples.

	Example 1	Example 2	
Parameter	$i = 1$	$i = 1$	$i = 2$
m_i (kg)	2.5	2.5	2.5
l_i (m)	0.26	0.26	0.26
ρ_i (m)	0.032	0.032	0.032
J_i (kg · m^2)	0.08	0.05	0.05
M_i (N · m)	1/3	0.2	0.2
F_i (N)	2.083	1.25	1.25
T_i (N · m)	16.93	16.25	16.25
L_i (m)	0.123	0.077	0.077
G_i (m/s^2)	0.7	0.469	0.273
κ_i (1/s^2)	3	3	3
r_{ij}^* (m)	0.443	0.407	0.407
k_i (1/s)	8.23	8.06	8.06
$\bar{\mu}_i$ (m/s^2)	1.56	0.938	0.938
η_i (m/s)	0.19	0.155	0.155
r_{ij} (m)	0.443	0.407	0.407
$\bar{r}_{ij}$ (m)	0.471	0.437	0.439
h_{ij} (m)	0.671	0.692	0.733
R_i (m)	0.75	0.75	0.75
r_ϵ (m)	0.453	0.408	0.408
θ_{ij} (rad)	0.040	0.070	0.076
Δ_{ij} (m)	0.2	0.255	0.294
K_{ij}^a (1/s^2)	0.341	0.491	2.554

while avoiding collisions with two static obstacles. The obstacles are located at $\mathbf{z}_2 = [-1.5 \text{ m} - \frac{d}{2}, 0 \text{ m}]^{\mathrm{T}}$ and $\mathbf{z}_3 = [1.5 \text{ m} + \frac{d}{2}, 0 \text{ m}]^{\mathrm{T}}$, where $d = 0.33$ m is the diameter—or largest dimension—of the obstacles and the vehicle. The trajectory tracking control is given by (10) for

$$\mathbf{g}_1(\tilde{\mathbf{z}}_1(t)) = \begin{cases} \kappa_1 \tilde{\mathbf{z}}_1(t), & \text{if } \|\tilde{\mathbf{z}}_1(t)\| \leq \frac{G_1}{\kappa_1} \\ G_1 \dfrac{\tilde{\mathbf{z}}_1(t)}{\|\tilde{\mathbf{z}}_1(t)\|}, & \text{otherwise} \end{cases} \tag{23}$$

after performing the input–output feedback linearization of Section 2.2.

We assume that the vehicle's sensing range is bounded by a radius of $R_1 = 0.75$ m and that the minimum safe distance that the vehicle may come from an obstacle is $r_{1j}^* = d + L_1 = 0.443$ m. We further assume that the vehicle's sensing process is subjected to a noise error $\mathbf{d}_1$ with uniform distribution in the set $\mathcal{Z}_1 = \{\mathbf{d}_1 : \mathbf{d}_1 \in \Re^2, \|\mathbf{d}_1\| \leq 0.2 \text{ m}\}$. The avoidance control is designed according to Theorem 4.1 with an avoidance radius of $r_{1j} = 0.443$ m.

Figure 3 depicts the evolution of the system. The vehicle, which is initialized at $[x_1(0), y_1(0), \phi_1(0)]^{\mathrm{T}} = [0 \text{ m}, 0 \text{ m}, \pi/2 \text{ rad}]^{\mathrm{T}}$, starts tracking the desired trajectory. It encounters the first obstacle at $t \approx 45$ s, when the obstacle enters its sensing region delimited by the dotted, blue circle. At this point, the vehicle starts diverging from the desired trajectory to avoid a potential collision with the first obstacle, $\mathbf{z}_2$. Once the obstacle is outside of the vehicle's sensing area, the vehicle is able to return to the desired trajectory as seen in Figure 3(c). The vehicle then encounters

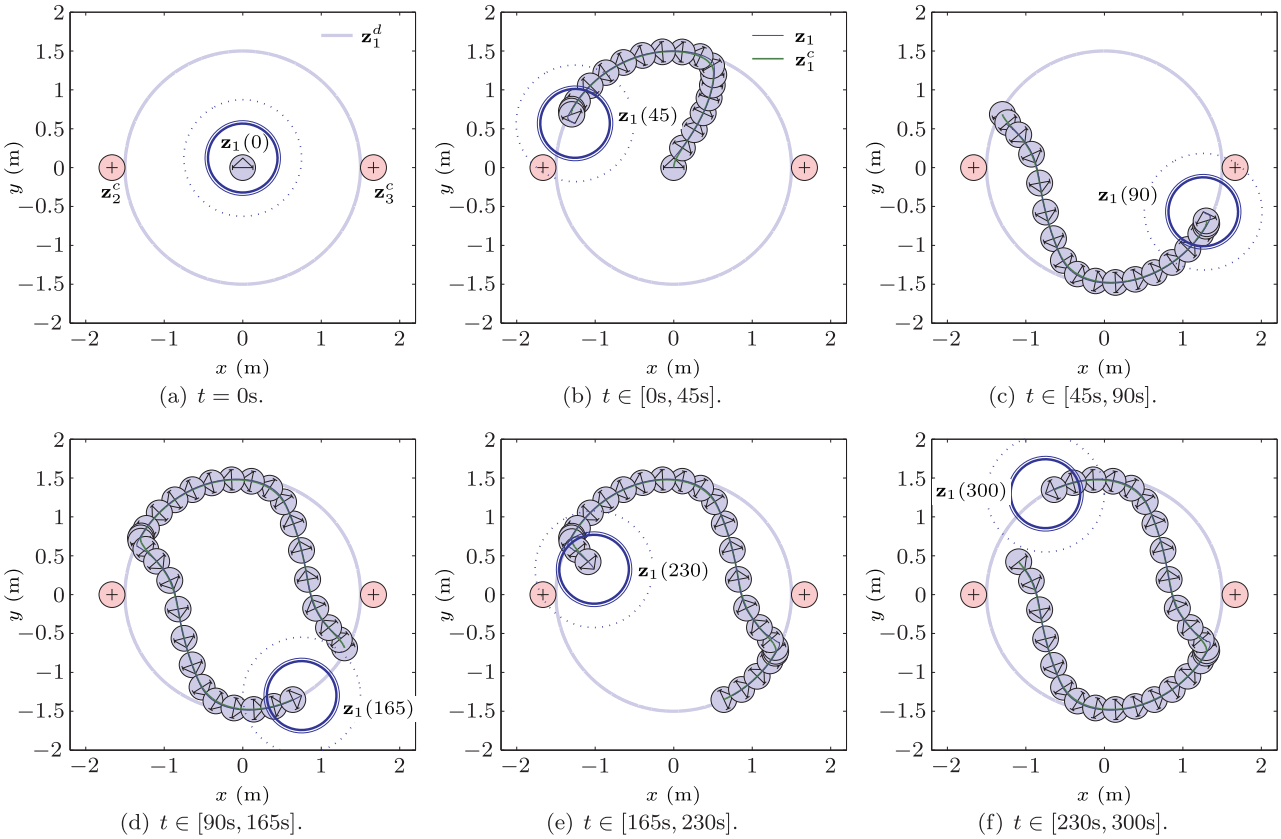

(a) $t = 0$s. (b) $t \in [0\text{s}, 45\text{s}]$. (c) $t \in [45\text{s}, 90\text{s}]$.

(d) $t \in [90\text{s}, 165\text{s}]$. (e) $t \in [165\text{s}, 230\text{s}]$. (f) $t \in [230\text{s}, 300\text{s}]$.

Fig. 3. Sequential motion of a single vehicle while interacting with two static obstacles. The position of the frontal reference point $\mathbf{z}_1$ and centroid $\mathbf{z}_1^c$ of the vehicle are traced by the fine blue and green lines, respectively. In addition, the position of the nonholonomic vehicle is marked by the blue-filled circles, with an inner triangle pointing in the vehicle's heading direction and with vertex at $\mathbf{z}_1$. Newer positions are over-imposed and time-spaced by 2.5 s. The position of the obstacles is marked by the light red circles with an inner cross. The reference trajectory is delineated by the bold, light blue line. The Detection, Conflict, and Avoidance regions at the end of each simulation interval are delimited by circles with dashed, fine, and bold blue lines, respectively.

the second obstacle at $t \approx 90$ s which starts avoiding to prevent a collision. The vehicle comes to the proximity of both obstacles several times during the simulation, avoiding collisions successfully every time (as seen in Figure 4(a)) and returning to the desired trajectory once the conflict has been resolved (see Figure 4(b)).

The evolution of the system's internal dynamics is traced in Figure 4(b). Note that $\phi_1(t)$ keeps increasing at a nearly constant rate (except at the instances when the vehicle detects an obstacle). This behavior is to be expected from the desired trajectory, which keeps shifting the heading of the vehicle to its left (toward the center of the circle).

The applied control torques at the wheels are illustrated in Figure 5. Observe that the control torques remain well below their limits of $M_i = 333.3$ mN for all time. Furthermore, for the most part of the simulation, the control torques approach zero and the wheels experience zero acceleration. This implies that the vehicle's wheels reach a constant velocity soon after solving the potential conflict, as should be expected from the vehicle's circular trajectory.

6.2. Example 2: Two cooperative vehicles

In the second example, we consider the interaction of two vehicles that must avoid collisions while both are tracking infinity-shaped trajectories given by

$$\mathbf{z}_1^d(t) = \left[3.0 \sin\left(\frac{\pi}{230}t\right) \text{ m}, 1.5 \sin\left(\frac{\pi}{230}t\right) \text{ m}\right]^{\mathrm{T}}$$

$$\mathbf{z}_2^d(t) = \left[-2.5 \sin\left(\frac{\pi}{230}t\right) \text{ m}, -1.25 \sin\left(\frac{\pi}{230}t\right) \text{ m}\right]^{\mathrm{T}}$$

The trajectory tracking control laws for the vehicles are computed according to (10) and (23) with control parameters listed in Table 1. Both vehicles implement the proposed cooperative avoidance control law, where we have assumed a sensing and antitarget radii of $R_1 = R_2 = 0.75$ m and $r_{12}^* = r_{21}^* = 0.407$ m, respectively. We further assume that the vehicles experience sensing detection delays and the effect of random measurement noise. Mathematically, the uncertainties can be characterized by

$$\mathbf{d}_{12}(t) = -\int_{t-T_1}^{t} \dot{\mathbf{z}}_2^c(\tau)\, d\tau + \boldsymbol{\zeta}_1(t),$$

$$\mathbf{d}_{21}(t) = -\int_{t-T_2}^{t} \dot{\mathbf{z}}_1^c(\tau)\, d\tau + \boldsymbol{\zeta}_2(t)$$

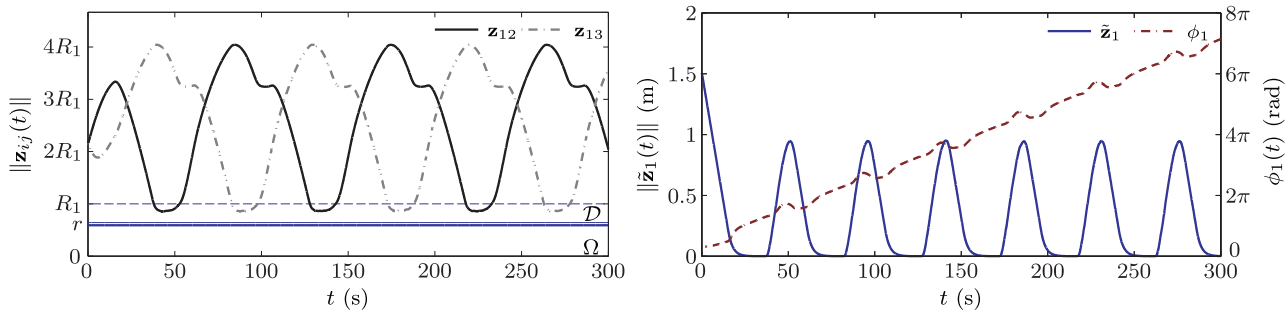

(a) Distances between vehicle and obstacles. (b) Tracking error and heading of vehicle.

Fig. 4. (a) The distances between the vehicle and the obstacles are traced by the solid black and dashed gray lines. The extent of the Detection and Avoidance regions is indicated by the dashed and solid blue lines, respectively. (b) The tracking error of the vehicle is illustrated by the solid, blue line, whereas the heading is traced by the dashed, dark, red line.

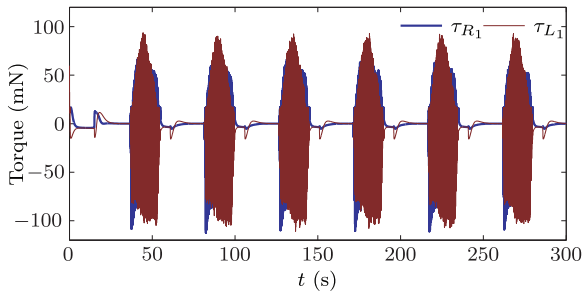

Fig. 5. Control torques τ_{R_1} and τ_{L_1}.

where $T_1 = 1.0$ s and $T_2 = 1.25$ s denote constant detection delays for the first and second vehicle, respectively, and $\boldsymbol{\zeta}_1$ and $\boldsymbol{\zeta}_2$ are random noises with uniform distribution on the set $\mathcal{Z} = \{\boldsymbol{\zeta}_i : \boldsymbol{\zeta}_i \in \Re^2, \|\boldsymbol{\zeta}_i\| \leq 0.1 \text{ m}\}$. The complete list of system and control parameters is given in Table 1.

The results of the simulation are illustrated in Figure 6 for $[x_1(0), y_1(0), \phi_1(0)]^{\mathrm{T}} = [-0.5\text{m}, -0.25\text{ m}, \pi/2 \text{ rad}]^{\mathrm{T}}$ and $[x_2(0), y_2(0), \phi_2(0)]^{\mathrm{T}} = [0.25\text{ m}, 0.25\text{ m}, -\pi/4 \text{ rad}]^{\mathrm{T}}$ as initial conditions. As soon as the simulation starts, the vehicles begin to move toward their desired trajectories, eventually entering each other's detection region. This activates their avoidance control strategies for the first time, which makes the vehicles slightly diverge from their desired trajectory in order to avoid a collision (see Figure 6(b) around $(x, y) = (0\text{ m}, 0\text{ m})$). Once the conflict has been resolved, i.e. the vehicles are outside of each other's sensing region, both vehicles are able to converge to their desired trajectories. As seen in Figures 6(c) to (e), the vehicles enter each other's detection region at two more instances ($t \approx 225$ s and $t \approx 450$ s). Yet, each time, they are able to avoid collisions and to return to their desired trajectory once they are safely apart. Figure 7(a) confirms that the vehicles never enter each other's Avoidance regions. Similarly, Figure 7(b) shows that the trajectory tracking errors converge to zero once the agents are safely apart. Furthermore, it shows that ϕ_i remain bounded for the given desired trajectory.

Finally, the applied control torques are plotted in Figure 8. Note that none of the control torques reach the saturation bound of $M_i = 200$ mN. Also observe that the control torques for the second vehicle were generally larger than for the first vehicle. This behavior responds to the use of larger (resp. lower) avoidance (resp. tracking) control authority by the second vehicle in comparison to the first robot.

7. Experiments

In addition to simulations, we also performed three different experiments on a pair of unmanned nonholonomic vehicles. The experimental results demonstrate the robustness and efficacy of the proposed control law.

7.1. Experimental testbed

The experimental tests were carried out in the Laboratory for Autonomous Robotics and Systems at the University of Texas at Dallas. The testbed consists of two iRobot Create vehicles, confined to a squared workspace of approximately 16 m^2 (see Figure 9), and a motion capture system dedicated to track the position and orientation of both robots. The iRobot Creates, which are illustrated in Figure 10, are two differential two-wheel drive robots with dynamics given as in (1) with parameters $m_i = 2.5$ kg, $J_i = 0.08$ kg $\cdot$ m^2, $\rho = 0.032$ m, $l_i = 0.26$ m, and $M_i = 0.33$ N $\cdot$ m. Each iRobot Create is equipped with a gumstix that allows it to communicate wirelessly with a PC (a custom built PC with an Intel Xeon E5430 quad-core processor with 2.66 GHz of speed). The PC computes the control commands for each vehicle using QuaRC and Simulink with an update rate of 50 Hz. The latency between the PC and the gumstix receivers is assumed to be negligible. Consequently, delays within each vehicle's feedback loop are considered to be sufficiently small and are ignored.

Position and orientation data for both vehicles are obtained using VICON's Motion Capture System. The motion capture system consists of multiple high speed cameras distributed around the workspace and capable of tracking position and orientation of the agents in real-time with a sub-millimeter accuracy at a sampling rate of 120 Hz.

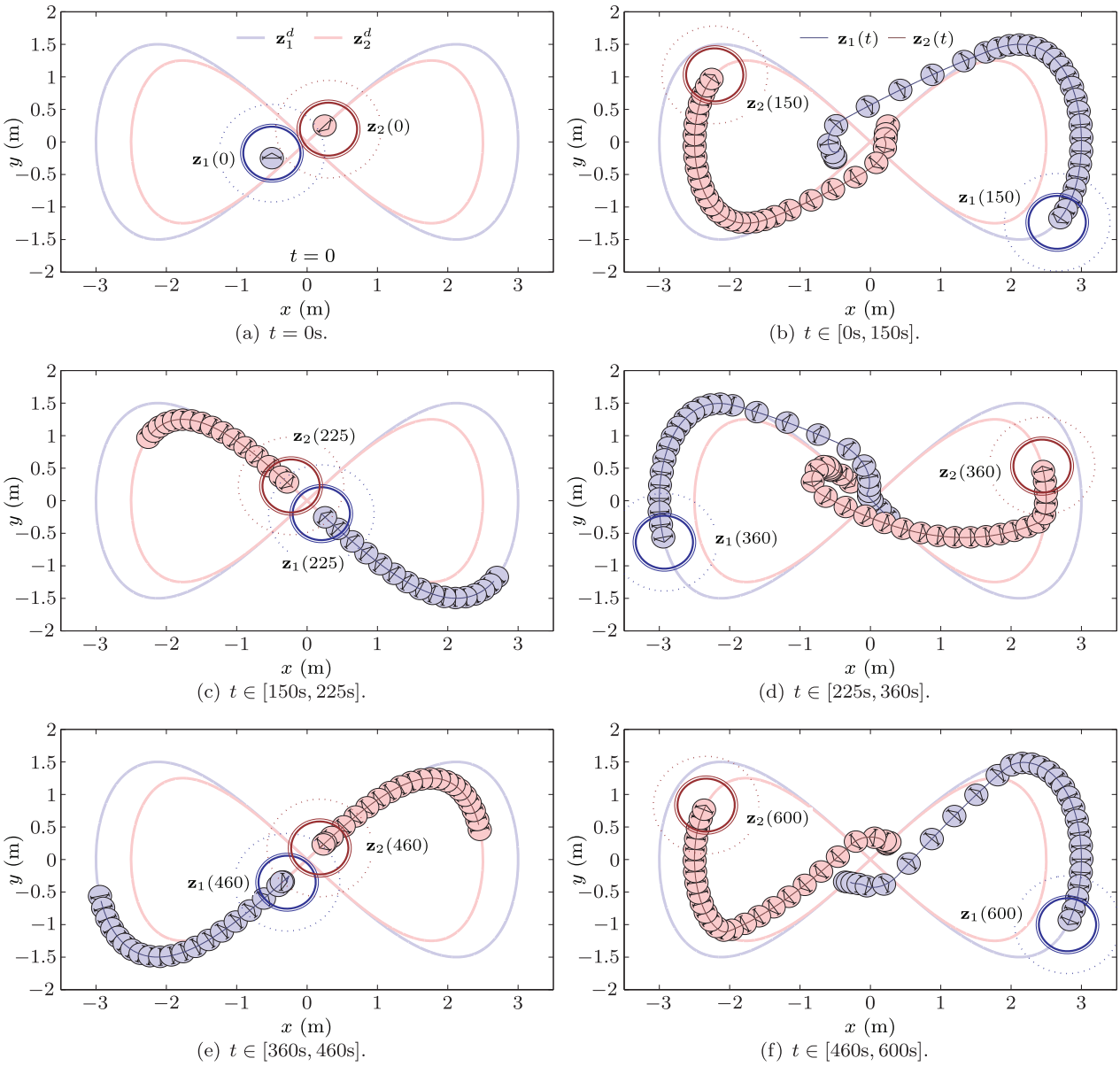

Fig. 6. Sequential motion of two vehicles in a cooperative scenario. The position of the frontal reference point $\mathbf{z}_i$ is traced by the fine blue line, for the first vehicle, and the dark red line, for the second. The positions of the nonholonomic vehicles are also marked by the blue-filled circles, for the first agent, and by the light, red-filled circles, for the second agent. The heading direction of the vehicles is indicated by the inner triangles with vertices located at $\mathbf{z}_i$. Newer positions are over-imposed and time-spaced by 5.0 s. The reference trajectories for the first and second vehicles are delineated by the bold, light blue and red lines, respectively. The Detection, Conflict, and Avoidance regions for both vehicles at the end of each simulation interval are delimited by circles with dashed, fine, and bold lines, respectively, centered at $\mathbf{z}_i$.

Position and orientation information from both vehicles is then transmitted to the main PC (see Figure 10) with low latency (less than 10 ms) such that every vehicle knows its own location. Velocities of the vehicles are then computed locally by differentiation.

Uncertainties in the sensing process of the other vehicle (i.e. $\mathbf{d}_{ij}(t)$) are artificially generated by the addition of a buffer that delays position information (refer to Figure 10 for an illustration). By artificially generating a delay, we are able to regulate and monitor the sensing error.

7.2. *Experiment 1: Trajectory tracking with noncooperative avoidance control*

In the first experiment, the vehicles are set to track concentric, circular trajectories delineated by

$$\mathbf{z}_1^d(t) = \left[1.2\cos\left(\frac{\pi}{40}t\right)\ \text{m}, 1.2\sin\left(\frac{\pi}{40}t\right)\ \text{m}\right]^{\mathrm{T}},$$
$$\mathbf{z}_2^d(t) = \left[1.0\cos\left(\frac{\pi}{40}t\right)\ \text{m}, -1.0\sin\left(\frac{\pi}{40}t\right)\ \text{m}\right]^{\mathrm{T}}$$

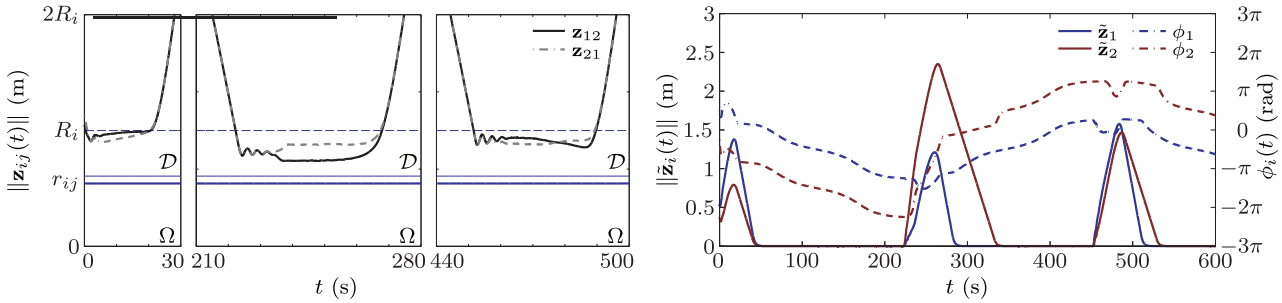

(a) Distances between the two vehicles. (b) Tracking error and heading of vehicles.

Fig. 7. (a) The distances between both vehicles, measured from $\mathbf{z}_i$ to $\mathbf{z}_j^c$, are traced by the solid black line ($(i,j) = (1,2)$) and dashed gray line ($(i,j) = (2,1)$). Note that, in general, $\mathbf{z}_{ij} \neq \mathbf{z}_{ji}$. The plot is divided in three discontinuous sets of time to illustrate only the intervals when the vehicles were in conflict. The extent of the Detection and Avoidance regions is indicated by the dashed and solid blue lines, respectively. (b) The tracking errors of the vehicles are illustrated by the solid lines, whereas the headings are traced by the dashed red lines.

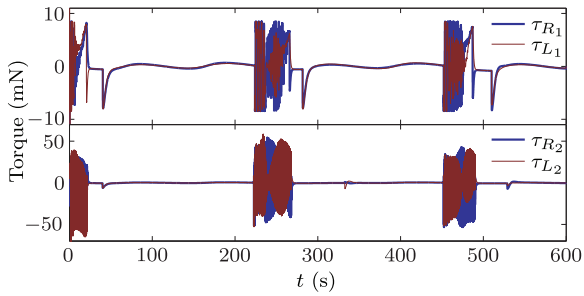

Fig. 8. Control torques τ_{R_i} and τ_{L_i}.

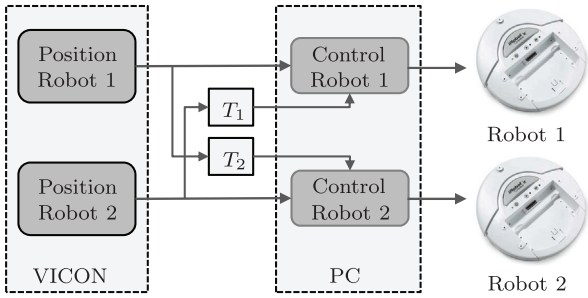

Fig. 10. Diagram of the testbed. The iRobot Creates are illustrated on the right side of the diagram.

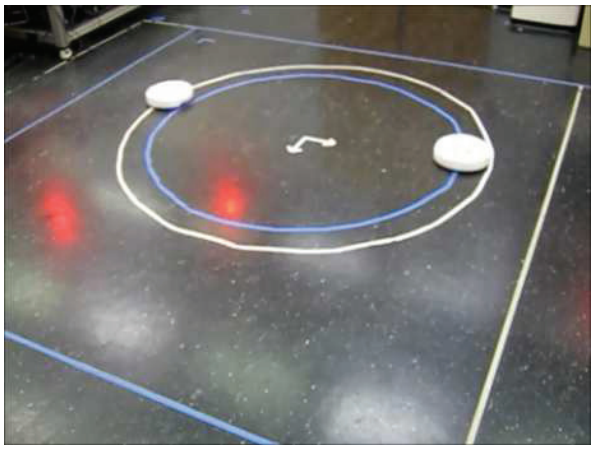

Fig. 9. Experimental workspace.

To converge to the desired trajectory, the vehicles implement the trajectory tracking control law of (10) and (23) for $G_1 = 0.787$ m/s^2 and $G_2 = 0.916$ m/s^2, and with other control parameters as listed in Table 2. The desired trajectories should expose the vehicles to a potential collision when they come close to the x-axis, where the distance between the desired trajectories is less than the antitarget radius (i.e. $\|\mathbf{z}_1^d - \mathbf{z}_2^d\| \to 0.20$ m $< r_{12}^*$).

Table 2. List of experimental control parameters.

	Experiment 1		Experiment 2	Experiment 3
Parameter	$i = 1$	$i = 2$	$i \in \{1,2\}$	$i \in \{1,2\}$
F_i (N)	2.083	2.083	2.083	2.083
T_i (N · m)	16.93	16.93	16.93	16.93
L_i (m)	0.123	0.123	0.123	0.123
κ_i (1/s^2)	6	6	6	6
r_{ij}^* (m)	0.443	–	0.443	0.443
k_i (1/s)	8.23	8.23	8.23	8.23
$\bar{\mu}_i$ (m/s^2)	1.56	1.56	1.56	1.56
η_i (m/s)	0.19	0.19	0.19	0.19
r_{ij} (m)	0.443	–	0.443	0.463
$\bar{r}_{ij}$ (m)	0.494	–	0.494	0.511
h_{ij} (m)	0.622	–	0.622	0.702
R_i (m)	0.80	–	0.80	0.75
θ_{ij} (rad)	0.090	–	0.090	0.090
Δ_{ij} (m)	0.128	–	0.128	0.191
K_{ij}^a (1/s^2)	0.069	–	0.069	0.694

We consider the case where only the first vehicle implements the proposed avoidance control law. The sensing radius of the vehicle is restricted to $R_1 = 0.800$ m, whereas the antitarget radius is set to $r_{12}^* = 0.443$ m. The error in the obstacle detection process of the first vehicle is owed

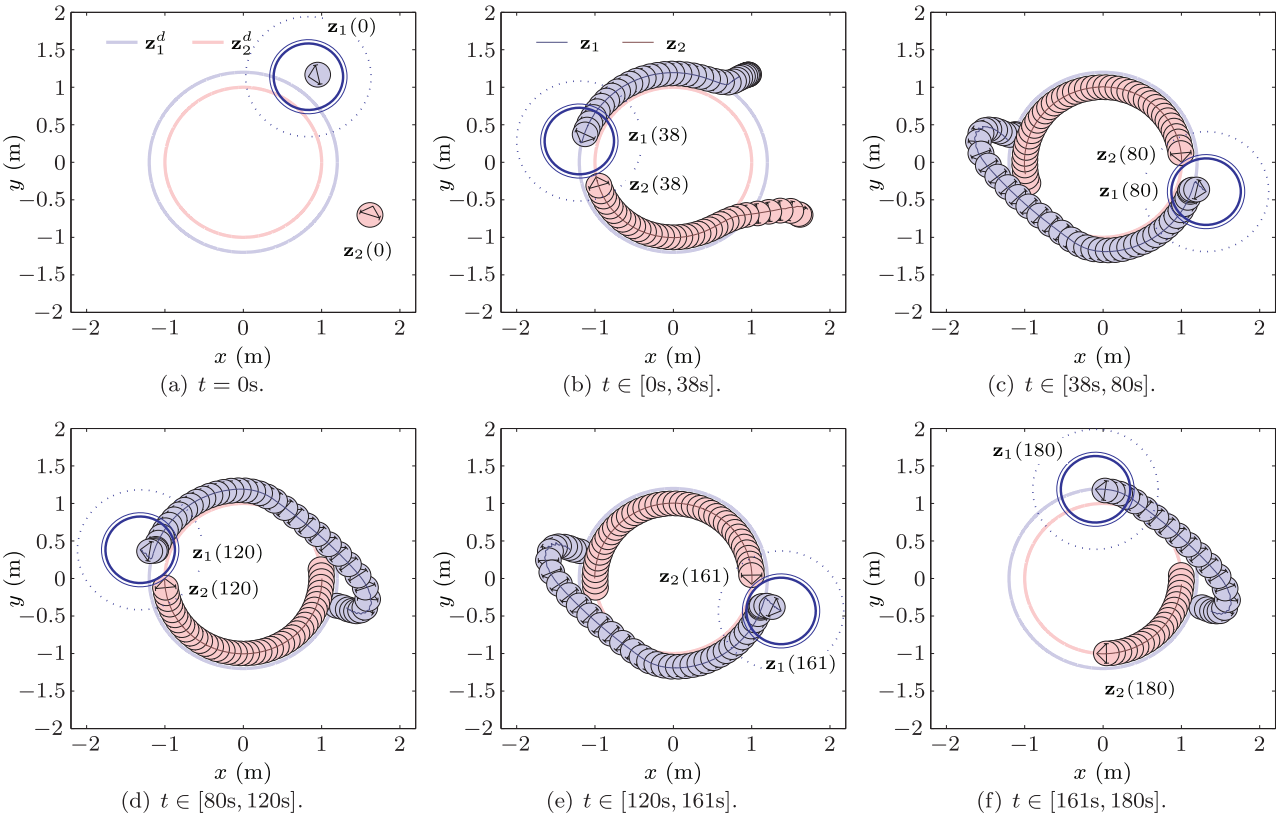

(a) $t = 0$s. (b) $t \in [0\text{s}, 38\text{s}]$. (c) $t \in [38\text{s}, 80\text{s}]$.

(d) $t \in [80\text{s}, 120\text{s}]$. (e) $t \in [120\text{s}, 161\text{s}]$. (f) $t \in [161\text{s}, 180\text{s}]$.

Fig. 11. Sequential motion of two vehicles in a noncooperative scenario. The position of the frontal reference point $\mathbf{z}_i$ is traced by the fine blue line, for the first vehicle, and the dark red line, for the second. The positions of the nonholonomic vehicles are also marked by the blue-filled circles, for the first agent, and by the light, red-filled circles, for the second agent. The heading direction of the vehicles is indicated by the inner triangles with vertices located at $\mathbf{z}_i$. Newer positions are over-imposed and time-spaced by 1.0 s. The reference trajectories for the first and second vehicles are delineated by concentric circles with bold, light blue and red lines, respectively. The Detection, Conflict, and Avoidance regions for the first vehicle at the end of each plotted interval of time are delimited by circles with dashed, fine, and bold blue lines, respectively, and centered at $\mathbf{z}_i$.

to a constant detection delay, $T_1 = 0.5$ s, which can be characterized as

$$\mathbf{d}_{12}(t) = -\int_{t-T_1}^{t} \dot{\mathbf{z}}_2^c(\tau)\, d\tau$$

Since the maximum linear velocity[6] of the second vehicle is regulated at 0.255 m/s, we can bound the sensing error by $\Delta_{12} = 0.128$ m. Having a bound on the uncertainty, we design the avoidance control according to Theorem 4.1. The complete set of control parameters is given in Table 2.

The experimental results are plotted in Figures 11 and 12. As illustrated in Figure 11(b), within the first few seconds, the vehicles are able to converge at their desired trajectories despite the fact that both vehicles started outside of their circular paths. They have the first encounter at $t \approx 35$ s, when the first vehicle activates the avoidance control (see Figure 11(b)). The first vehicle is able to resolve the conflict and avoid a collision by shifting to the left side of the workspace, allowing the second vehicle to continue its path (see Figure 11(c)). Once the second vehicle is outside of the sensing region, the first vehicle is able to converge to the desired trajectory. The vehicles arrive at a conflict once again at $t \approx 75$ s, $t \approx 115$ s, and $t \approx 155$ s. Yet, the first vehicle is able to resolve the conflict, avoid a collision, and return to its path each time.

Figure 12(a), which plots the distance between both vehicles as a function of time, shows that the second vehicle never entered the first vehicle's Avoidance region. Similarly, Figure 12(b) shows that the second vehicle was able to track satisfactorily the desired trajectory at all times, while the first agent did the same whenever the second vehicle was safely apart.

7.3. *Experiment 2: Trajectory tracking with cooperative avoidance control*

The second experiment studies the case where both vehicles implement the proposed avoidance control. We choose the same desired trajectories and control parameters as in Experiment 1 (refer to Table 2 for the complete set of

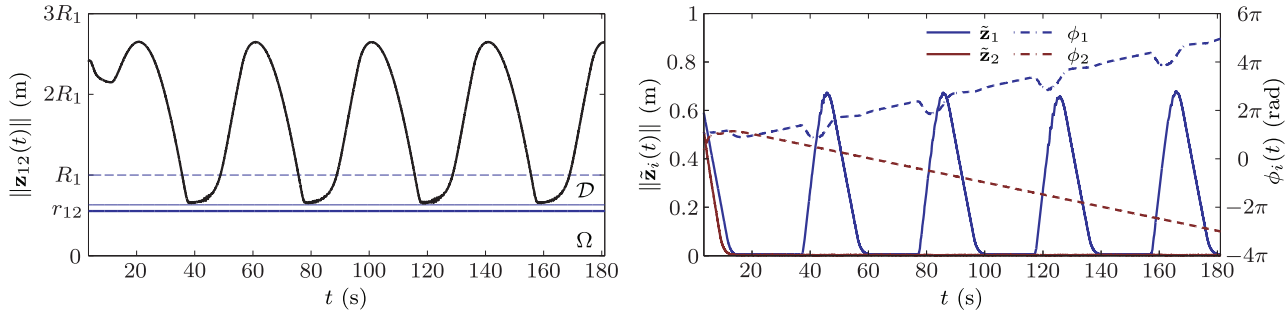

(a) Distance between the two vehicles. (b) Tracking error and heading of vehicles.

Fig. 12. (a) The distance between both vehicles, measured from $\mathbf{z}_1$ to $\mathbf{z}_2^c$. The extent of the Detection, Conflict, and Avoidance regions is indicated by the dashed, solid-fine, and solid-bold blue lines, respectively. (b) The tracking errors of the vehicles are illustrated by the solid lines, whereas the headings are traced by the dashed red lines.

control parameters). We also choose similar sources of sensing uncertainties for both vehicles

$$\mathbf{d}_{12}(t) = -\int_{t-T_1}^{t} \dot{\mathbf{z}}_2^c(\tau)\,d\tau, \quad \mathbf{d}_{21}(t) = -\int_{t-T_2}^{t} \dot{\mathbf{z}}_1^c(\tau)\,d\tau \tag{24}$$

where $T_1 = T_2 = 0.5$ s are constant sensing delays. The avoidance control laws are then designed according to Theorem 4.1 (see Table 2 for the list of control parameters).

Figure 13 depicts the interaction of both vehicles over time. Both vehicles start outside of their circular paths but converge within the first 10 s to their desired trajectories. They enter each other's detection region at $t \approx 35$ s, at which point, both vehicles initiate their avoidance strategies. The vehicles react by first stopping and then bouncing with each other while moving to opposite sides. The short-lived bouncing—illustrated more clearly in Figure 14(a) when the vehicles are at the closest distance from each other—is caused by the sensing delay. Once the vehicles are safely apart, they are able to retake their course toward their desired trajectories (see Figure 13(c)). The vehicles encounter each other at $t \approx 75$ s, $t \approx 115$ s, and $t \approx 155$ s. Each time, they avoid a collision by repeating the same resolution behavior.

The distances between both vehicles, measured from $\mathbf{z}_i$ to $\mathbf{z}_j^c$, are illustrated in Figure 14(a). Observe that the vehicles never enter the Avoidance region. Similarly, Figure 14(a) plots the trajectory tracking error and the evolution of the internal dynamics for both agents. Observe that the tracking errors converge to zero whenever the vehicles are safely apart. The internal states ϕ_i, on the other hand, grow at constant rates.

7.4. *Experiment 3: Set-point stabilization with cooperative avoidance control*

The last experiment consists of commanding the vehicles toward opposite corners of a square, which is a set-point regulation problem. The desired position for the first and second vehicle are $\mathbf{z}_1^d(t) = -\mathbf{z}_2^d(t) = [1.25\text{ m}, 1.25\text{ m}]^{\mathrm{T}}$. To achieve their objectives, the vehicles implement the tracking control law of (10) and (23) for $G_i = \bar{\mu}_i = 1.563$ N and control parameters as listed in Table 2. To avoid collisions, both vehicles implement the proposed cooperative avoidance control law. We choose sensing and antitarget radii of 0.75 m and 0.443 m, respectively, and delay the vehicles' obstacle detection process by 1.0 s such that the sensing uncertainties can be characterized as in (24) for $T_i = 1.0$ s.

The experimental results are presented in Figure 15 and 16. The vehicles, which are initialized at opposite corners of the squared-area, start moving toward their desired positions according to their tracking control law until they enter each other's detection regions at $t \approx 12$ s (see Figure 15(b)). As the vehicles come closer, they first react by reducing their velocities and, then, by moving slightly in opposite directions. Observe that they exhibit a bouncy behavior while in conflict due to the sensing delay in the localization process (see the fine blue and dark-red lines in Figure 15(c), which trace continuously the position of $\mathbf{z}_1$ and $\mathbf{z}_2$, respectively, as well as the oscillatory behavior in Figure 16(a)). Once the vehicles are at a safe distance from each other and their localizations do not interfere with each other's desired paths, the agents are able to converge to their desired position. Figure 16(a) confirms that the vehicle never entered the Avoidance region.

Figure 16(b) illustrates the position error and the heading of both vehicles. Note that the agents were able to converge to their desired positions and that the headings stabilized at constant angles as expected from Theorem 3.2. Moreover, note the symmetric behavior between both vehicles with nearly identical position errors and opposite headings.

8. Conclusion

In this paper, we have studied two problems related to the motion control of dynamic nonholonomic systems of unicycle type. The first problem was the stabilization and trajectory tracking control of a dynamic nonholonomic vehicle with saturated control inputs. The second problem addressed the design of control strategies to guarantee

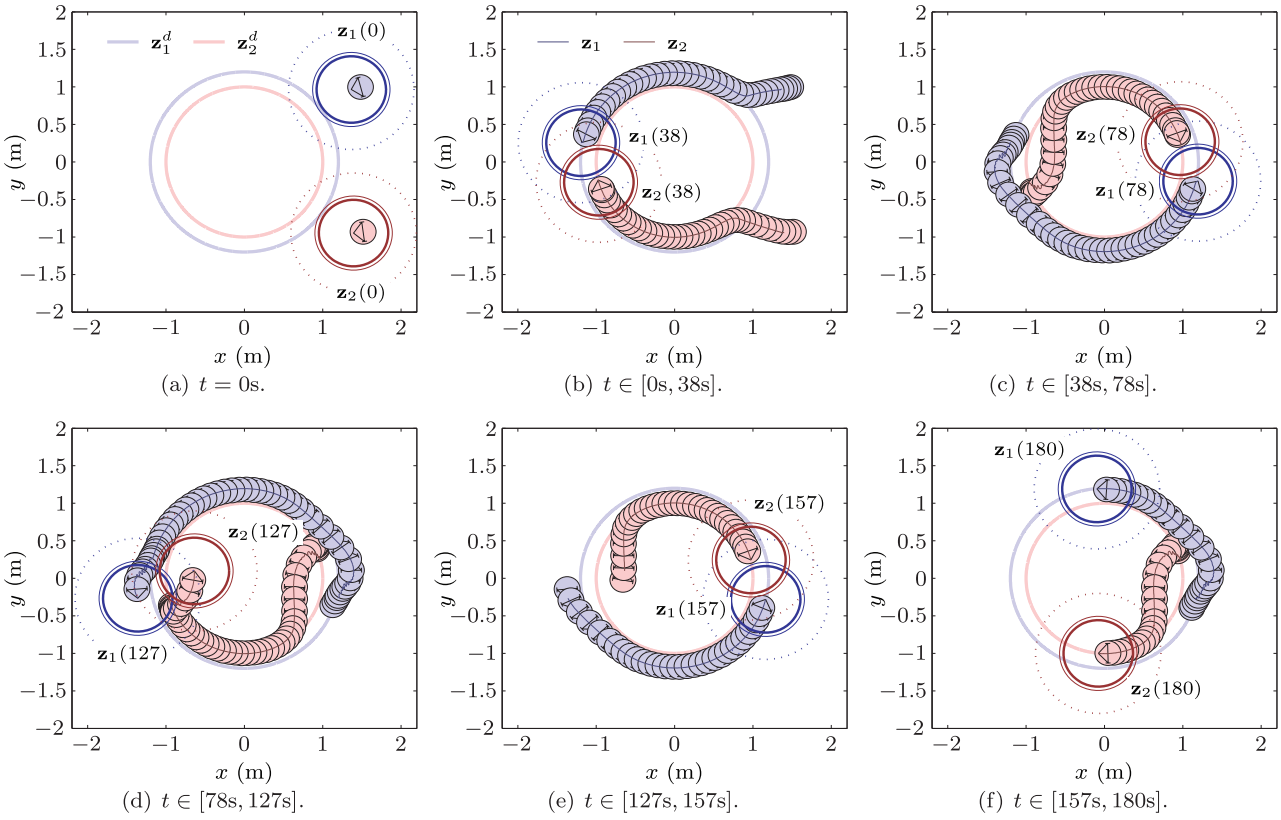

(a) $t = 0$s. (b) $t \in [0\text{s}, 38\text{s}]$. (c) $t \in [38\text{s}, 78\text{s}]$.

(d) $t \in [78\text{s}, 127\text{s}]$. (e) $t \in [127\text{s}, 157\text{s}]$. (f) $t \in [157\text{s}, 180\text{s}]$.

Fig. 13. Sequential motion of two vehicles in a cooperative scenario. The position of the frontal reference point $\mathbf{z}_i$ is traced by the fine blue line, for the first vehicle, and the dark red line, for the second. The positions of the nonholonomic vehicles are also marked by the blue-filled circles, for the first agent, and by the light, red-filled circles, for the second agent. Newer positions are over-imposed and time-spaced by 1.0 s. The reference trajectories for the first and second vehicles are delineated by the concentric circles with bold, light blue and red lines, respectively. The Detection, Conflict, and Avoidance regions for both vehicles at the end of each plotted interval of time are delimited by circles with dashed, fine, and bold lines, respectively, centered at $\mathbf{z}_i$.

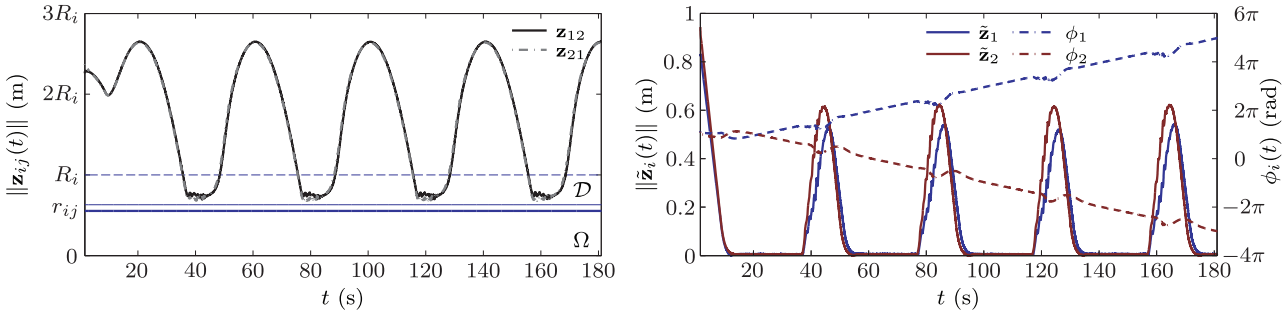

(a) Distances between the two vehicles. (b) Tracking error and heading of vehicles.

Fig. 14. (a) The distances between both vehicles, measured from $\mathbf{z}_i$ to $\mathbf{z}_j^c$, are traced by the solid black line ($(i,j) = (1,2)$) and dashed gray line ($(i,j) = (2,1)$). Note that, in general, $\mathbf{z}_{ij} \neq \mathbf{z}_{ji}$. The extent of the Detection, Conflict, and Avoidance regions is indicated by the dashed, solid-fine, and solid-bold blue lines, respectively. (b) The tracking errors of the vehicles are illustrated by the solid lines, whereas the headings are traced by the dashed red lines.

collision-free transit between two nonholonomic vehicles with acceleration constraints and obstacle detection errors. Using Lyapunov-based analysis and avoidance functions, we were able to develop solutions for both problems.

First, we showed that by using a bounded input–output feedback linearization control law (Lawton et al., 2003) along with an appropriate bounded trajectory tracking control strategy, we can guarantee convergence of the linearized system to the desired trajectory whenever the vehicle is not in a collision threat and provided analytical bounds on the vehicle's admissible velocity and acceleration. Moreover, we proved that the internal dynamics are stable and

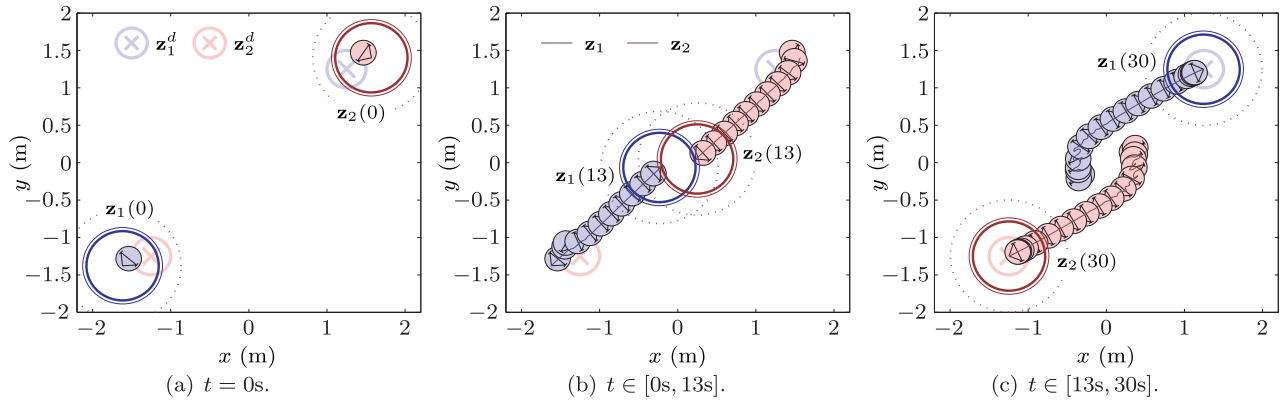

(a) $t = 0$s. (b) $t \in [0\text{s}, 13\text{s}]$. (c) $t \in [13\text{s}, 30\text{s}]$.

Fig. 15. Sequential motion of two vehicles in a cooperative scenario with set-point control law. The position of the reference point $\mathbf{z}_i$ is traced by the fine blue line, for the first vehicle, and the dark red line, for the second. The positions of the nonholonomic vehicles are also marked by the blue-filled circles, for the first agent, and by the light, red-filled circles, for the second agent. Newer positions are over-imposed and time-spaced by 1.0 s. The desired set-point for the first and second vehicle are marked by the circles with an inner cross. The Detection, Conflict, and Avoidance regions for both vehicles at the end of each plotted interval of time are delimited by circles with dashed, fine, and bold lines, respectively, centered at $\mathbf{z}_i$.

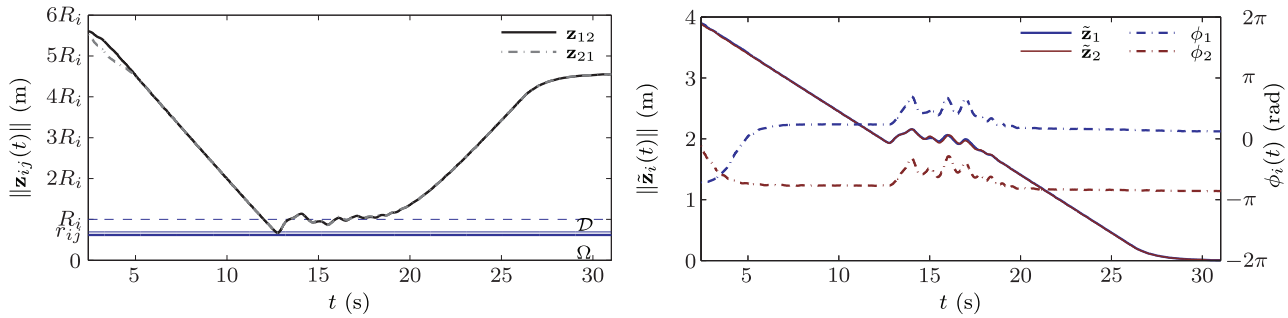

(a) Distances between the two vehicles. (b) Tracking error and heading of vehicles.

Fig. 16. (a) The distances between both vehicles, measured from $\mathbf{z}_i$ to $\mathbf{z}_j^c$, are traced by the solid black line ($(i,j) = (1,2)$) and dashed gray line ($(i,j) = (2,1)$). Note that, in general, $\mathbf{z}_{ij} \neq \mathbf{z}_{ji}$. The extent of the Detection, Conflict, and Avoidance regions is indicated by the dashed, solid-fine, and solid-bold blue lines, respectively. (b) The tracking errors of the vehicles are illustrated by the solid lines, whereas the headings are traced by the dashed red lines.

that the heading of the vehicle converges to a constant value when the reference trajectory is constant (i.e. a set-point). Next, we synthesized the tracking control law with a reactive collision avoidance strategy designed to accommodate for obstacle detection errors (e.g. errors due to delays, noise, and quantization) as well as limited sensing range. We developed strategies for the noncooperative and cooperative case and showed, via Lyapunov-based analysis, that if the vehicles start outside of each other's bounded conflict regions (a design parameter), then the vehicles are guaranteed to remain safely apart for all future times independently of conflicts between their desired trajectories. The resulting synthesized control law demands low computation, as it does not require complex online optimization or prediction techniques, and can be implemented in a decentralized arrangement (the vehicle does not need to know the control objectives of other agents, nor their position whenever they are outside of the vehicle's sensing region). Finally, we validated the overall control law via numerical simulations and experimental tests with two nonholonomic vehicles with saturated control inputs and bounded sensing errors. The results demonstrated that the control laws are robust to sensing uncertainties and are effective in guaranteeing trajectory tracking and collision avoidance.

In future work, we would like to extend the proposed control ideas to the general case of multiple vehicles and to systems with other kinematic or dynamic restrictions (e.g. vehicles with constant or non-zero velocity). Similarly, we would like to examine the application of time-varying and discontinuous control laws (e.g. Pomet, 1992; Astolfi, 1996; Oriolo et al., 2002) to achieve full-state asymptotic stability of wheeled mobile robots with dynamic models.

Funding

This research was partially supported by the National Science Foundation Grant ECCS 07-25433 and by the University of Texas at Dallas.

Notes

1. By agent we mean either a vehicle or an obstacle.
2. In what follows, we will omit time dependency of variables except when considered necessary.
3. The uncontrollability of ϕ limits the scope of the proposed strategy since many applications will require tight control of the vehicle's orientation for proper use of sensors (e.g. cameras with limited field of view) and other actuators (e.g. mounted arms). However, it is worth mentioning that in some applications, including surveillance, recognition, and navigation, we might be solely interested in the path (or area) traveled (or covered) by the agent regardless of the vehicle's orientation.
4. Throughout this work, we will name any obstacle or vehicle in the vicinity of the *i*th vehicle as the *j*th agent.
5. In contrast to the radius of the Antitarget region (which is given as part of the problem), the radius of the Avoidance region is chosen as a design parameter. For safety reasons, it is common in real applications to enforce a desired distance between vehicle and obstacle larger than the absolute minimum distance r_{ij}^{*}.
6. Recall that the collision avoidance control is computed by taking the distance of the first vehicle to the centroid of the second vehicle, $\mathbf{z}_2^c$. Therefore, we must take into consideration the maximum velocity at the centroid and not at the frontal reference point, $\mathbf{z}_2$.

References

Aguiar AP, Atassi AN and Pascoal AM (2000) Regulation of a nonholonomic dynamic wheeled mobile robot with parametric modeling uncertainty using Lyapunov functions. In: *Proceedings of the IEEE conference on decision control (CDC)*, Sydney, Australia, 12–15 December 2000, pp. 2995–3000.

Althoff D, Kuffner JJ, Wollherr D, et al. (2012) Safety assessment of robot trajectories for navigation in uncertain and dynamic environments. *Autonomous Robots* 32(3): 285–302.

Astolfi A (1996) Discontinuous control of nonholonomic systems. *Systems Control Letters* 27(1): 37–45.

Bloch AM and McClamroch NH (1989) Control of mechanical systems with classical nonholonomic constraints. In: *Proceedings of the IEEE conference on decision control (CDC)*, Tampa, FL, USA, 13–15 December 1989, pp. 201–205.

Bogue R (2012) Robots for space exploration. *Industrial Robot* 39(4): 323–328.

Brockett RW (1983) Asymptotic stability and feedback stabilization. In: Brockett RW, Millman RS and Sussmann HJ (eds) *Differential Geometric Control Theory*. Boston, MA: Birkhauser, pp. 181–191.

Campion G, D'Andrea Novel B and Bastin G (1991) Controllability and state feedback stabilizability of non holonomic mechanical systems. In: Canudas de Wit C (ed) *Advanced Robot Control* (*Lecture Notes in Control and Information Sciences*, Vol. 162). Berlin; Heidelberg, Germany: Springer, pp. 106–124.

Canudas de Wit C and Roskam R (1991) Path following of a 2-DOF wheeled mobile robot under path and input torque constraints. In: *Proceedings of the IEEE international conference on robotics and automation (ICRA)* Sacramento, CA, USA, pp. 1142–1147.

Canudas de Wit C and Sørdalen OJ (1992) Exponential stabilization of mobile robots with nonholonomic constraints. *IEEE Transactions on Automation and Control* 37(11): 1791–1797.

Chen H, Wang C, Yang L, et al. (2012) Semiglobal stabilization for nonholonomic mobile robots based on dynamic feedback with inputs saturation. *Journal of Dynamic Systems, Measurement, and Control* 134(4): 041006-1-8.

Cole DT, Goktogan AH, Thompson P, et al. (2009) Mapping and tracking. *IEEE Robotics and Automation Magazine* 16(2): 22–34.

Consolini L, Morbidi F, Prattichizzo D and Tosques M (2008) Leader–follower formation control of nonholonomic mobile robots with input constraints. *Automatica* 44(5): 1343–1349.

D'Andréa Novel B, Campion G, et al. (1995) Control of nonholonomic wheeled mobile robots by state feedback linearization. *International Journal of Robotics Research* 14(6): 543–559.

De La Cruz C and Carelli R (2008) Dynamic model based formation control and obstacle avoidance of multi-robot systems. *Robotica* 26: 345–356.

Do KD (2008) Formation tracking control of unicycle-type mobile robots with limited sensing ranges. *IEEE Transactions on Control Systems Technology* 16(3): 527–538.

Do KD (2009) Output-feedback formation tracking control of unicycle-type mobile robots with limited sensing ranges. *Robotics and Autonomous Systems* 57(1): 34–47.

Do KD, Jiang ZP and Pan J (2004) A global output-feedback controller for simultaneous tracking and stabilization of unicycle-type mobile robots. *IEEE Transactions on Robotics and Automation* 20(3): 589–594.

Elfes A (1989) Using occupancy grids for mobile robot perception and navigation. *IEEE Computer* 22(6): 46–57.

Fiorini P and Shiller Z (1998) Motion planning in dynamic environments using velocity obstacles. *International Journal of Robotics Research* 17(7): 760–772.

Fraichard T and Asama H (2003) Inevitable collision states: A step towards safer robots? In: *Proceedings of the IEEE/RSJ international conference on intelligent robots and systems (IROS)*, Las Vegas, NV, USA, 27–31 October 2003, pp. 388–393.

Frew E and Sengupta R (2004) Obstacle avoidance with sensor uncertainty for small unmanned aircraft. In: *Proceedings of the IEEE conference on decision control (CDC)*, Paradise Island, Bahamas, pp. 614–619.

Fulgenzi C, Spalanzani A and Laugier C (2007) Dynamic obstacle avoidance in uncertain environment combining PVOs and occupancy grid. In: *Proceedings of the IEEE international conference on robotics and automation (ICRA)*, Roma, Italy, 10–14 April 2007, pp. 1610–1616.

John A Volpe National Transportation Systems Center (2001) Vulnerability assessment of the transportation infrastructure relying on the Global Positioning System. Technical Report NAV-CEN, NTSC, U.S. Department of Transportation.

Khalil HK (2002) *Nonlinear Systems*. Upper Saddle River, NJ: Prentice Hall.

Khatib O (1986) Real-time obstacle avoidance for manipulators and mobile robots. *International Journal of Robotics Research* 5(1): 90–98.

Kinsey JC, Eustice RM and Whitcomb LL (2006) A survey of underwater vehicle navigation: Recent advances and new challenges. In: *Proceedings of the IFAC conference on the*

manoeuvring and control of marine craft, Lisbon, Portugal, 20–22 September 2006, pp. 1–12.

Kolmanovsky I and McClamroch NH (1995) Developments in nonholonomic control problems. *IEEE Control Systems Magazine* 15(6): 20–36.

Koren Y and Borenstein J (1991) Potential field methods and their inherent limitations for mobile robot navigation. In: *Proceedings of the IEEE international conference on robotics and automation (ICRA)*, Sacramento, CA, USA, 9–11 April 1991, pp. 1398–1404.

Kowalczyk W, Kozlowski K and Tar JK (2010) Trajectory tracking for multiple unicycles in the environment with obstacles. In: *Proceedings of RAAD*, Budapest, Hungary, 23–25 June 2010, pp. 451–456.

Kumar V and Michael N (2012) Opportunities and challenges with autonomous micro aerial vehicles. *International Journal of Robotics Research* 31(11): 1279–1291.

Lalish E and Morgansen KA (2012) Distributed reactive collision avoidance. *Autonomous Robots* 32(3): 207–226.

Lalish E, Morgansen KA and Tsukamaki T (2008) Decentralized reactive collision avoidance for multiple unicycle-type vehicles. In: *Proceedings of the American control conference*, Seattle, WA, USA, 11–13 June 2008, pp. 5055–5061.

Lamiraux F, Bonnafous D and Lefebvre O (2004) Reactive path deformation for nonholonomic mobile robots. *IEEE Transactions on Robotics* 20(6): 967–977.

Lawton JRT, Beard RW and Young BJ (2003) A decentralized approach to formation maneuvers. *IEEE Transactions on Robotics and Automation* 19(6): 933–941.

Leitmann G and Skowronski J (1977) Avoidance control. *Journal of Optimization Theory and Applications* 23(4): 581–591.

Leonard NE, Paley DA, Lekien F, et al. (2007) Collective motion, sensor networks, and ocean sampling. *Proceedings of the IEEE* 95(1): 48–74.

Loizou SG and Kyriakopoulos KJ (2008) Navigation of multiple kinematically constrained robots. *IEEE Transactions on Robotics* 24(1): 221–231.

Mastellone S, Stipanović DM, Graunke CR, et al. (2008) Formation control and collision avoidance for multi-agent nonholonomic systems: Theory and experiments. *International Journal of Robotics Research* 27(1): 107–126.

Moravec HP (1988) Sensor fusion in certainty grids for mobile robots. *AI Magazine* 9(2): 61–74.

Morin P and Samson C (2009) Control of nonholonomic mobile robots based on transverse function approach. *IEEE Transactions on Robotics* 25(5): 1058–1073.

Oikonomopoulos AS, Loizou SG and Kyriakopoulos KJ (2009) Coordination of multiple non-holonomic agents with input constraints. In: *Proceedings of the IEEE international conference on robotics and automation (ICRA)*, Kobe, Japan, 12–17 May 2009, pp. 869–874.

Oriolo G, De Luca A and Vendittelli M (2002) WMR control via dynamic feedback linearization: Design, implementation, and experimental validation. *IEEE Transactions on Control Systems Technology* 10(6): 835–852.

Palafox OM and Spong MW (2009) Bilateral teleoperation of a formation of nonholonomic mobile robots under constant time delay. In: *Proceedings of the IEEE/RSJ international conference on intelligent robots and systems (IROS)*, St. Louis, MO, 11–15 October 2009, pp. 2821–2826.

Pomet JB (1992) Explicit design of time-varying stabilizing control laws for a class of controllable systems without drift. *Systems and Control Letters* 18(2): 147–158.

Pomet JB, Thuilot B, Bastin G, et al. (1992) A hybrid strategy for the feedback stabilization of nonholonomic mobile robots. In: *Proceedings of the IEEE international conference on robotics and automation (ICRA)*, Nice, France, 12–14 May 1992, pp. 129–134.

Rockafellar RT (1966) Characterization of the subdifferentials of convex functions. *Pacific Journal of Mathematics* 17(3): 497–510.

Rockafellar RT (1968) Integrals which are convex functionals. *Pacific Journal of Mathematics* 24(3): 525–539.

Rodríguez-Seda EJ (2014) Decentralized trajectory tracking with collision avoidance control for teams of unmanned vehicles with constant speed. In: *Proceedings of the American control conference*, 4–6 June 2014.

Rodríguez-Seda EJ and Spong MW (2012) Guaranteed safe motion of multiple Lagrangian systems with limited actuation. In: *Proceedings of the IEEE conference on decision control (CDC)*, Maui, HI, USA, 10–13 December 2012, pp. 2773–2780.

Rodríguez-Seda EJ and Stipanović DM (2013) Guaranteed collision avoidance with discrete observations and limited actuation. In: Chen Y and Li L (eds) *Advances in Intelligent Vehicles*. Oxford: Academic Press, pp. 89–110.

Rodríguez-Seda EJ, Stipanović DM and Spong MW (2011a) Collision avoidance control with sensing uncertainties. In: *Proceedings of the American control conference*, San Francisco, CA, USA, 29 June–1 July 2011, pp. 3363–3368.

Rodríguez-Seda EJ, Stipanović DM and Spong MW (2011b) Lyapunov-based cooperative avoidance control for multiple Lagrangian systems with bounded sensing uncertainties. In: *Proceedings of the IEEE conference on decision control (CDC)*, Orlando, FL, USA, 12—15 December 2011, pp. 4207–4213.

Samson C (1995) Control of chained systems application to path following and time-varying point-stabilization of mobile robots. *IEEE Transactions on Automation and Control* 40(1): 64–77.

Sarkar N, Yun X and Kumar V (1994) Control of mechanical systems with rolling constraints: Application to dynamic control of mobile robots. *International Journal of Robotics Research* 13(1): 55–69.

Snape J, van den Berg J, Guy SJ, et al. (2011) The hybrid reciprocal velocity obstacle. *IEEE Transactions on Robotics* 27(4): 696–706.

Sørdalen OJ and Egeland O (1995) Exponential stabilization of nonholonomic chained systems. *IEEE Transactions on Automatic Control* 40(1): 35–49.

Stipanović DM, Hokayem PF, Spong MW, et al. (2007) Cooperative avoidance control for multiagent systems. *Journal of Dynamic Systems, Measurement, and Control* 129: 699–707.

Wurman PR, D'Andrea R and Mountz M (2008) Coordinating hundreds of cooperative, autonomous vehicles in warehouses. *AI Magazine* 29(1): 9–20.

Yamamoto Y and Yun X (1994) Coordinating locomotion and manipulation of a mobile manipulator. *IEEE Transactions on Automation and Control* 39(6): 1326–1332.

Appendix A. Symbol definition

The following is a list of symbols and definitions frequently used throughout the text. Note that Sections 2, 3, and 5 do not follow the *i*-subscript notation listed below.

$\mathbf{d}_{ij}$	Uncertainty in the location of the jth agent
$\mathcal{D}_{ij}$	ith vehicle's Detection region
f_i	Control force input
F_i	Maximum magnitude of f_i
$\mathbf{g}_i$	Tracking control vector function
G_i	Design parameter for tracking control
h_{ij}	$\bar{r}_{ij} + \delta_{ij}$
J_i	Moment of inertia
k_i	Constant gain
l_i	Distance between both vehicle's wheels
L_i	Positive constant, distance between the centroid and reference frontal point of the ith vehicle
m_i	Mass of the ith vehicle
M_i	Maximum magnitude of τ_{Li} and τ_{Ri}
r_{ij}	Radius of Avoidance region
r^*_{ij}	Radius of Antitarget region
$\bar{r}_{ij}$	Radius of Conflict region
R_i	Radius of Detection region
r_ϵ	$r_{ij} + \epsilon$
T_i	Maximum magnitude of τ_i
$\mathbf{u}_i$	New control input for the input–output feedback linearized vehicle
$\mathbf{u}^a_i$	Avoidance control law
$\mathbf{u}^o_i$	Trajectory tracking control law
$\mathcal{T}_{ij}$	ith vehicle's Antitarget region
v_i	Linear velocity
$\mathcal{W}_{ij}$	ith vehicle's Conflict region
x_i	Position of ith vehicle's centroid along the x-axis
y_i	Position of ith vehicle's centroid along the y-axis
$\mathbf{z}_i$	Cartesian coordinates of the input–output feedback linearized vehicle
$\mathbf{z}^c_i$	$[x_i, y_i]^{\mathrm{T}}$, position vector
$\mathbf{z}^d_i$	Desired trajectory for the input–output feedback linearized vehicle
$\tilde{\mathbf{z}}_i$	$\mathbf{z}_i - \mathbf{z}^d_i$, trajectory tracking error
$\mathbf{z}_{ij}$	$\mathbf{z}_i - \mathbf{z}^c_j$, distance between both agents
$\hat{\mathbf{z}}_{ij}$	$\mathbf{z}_i - \hat{\mathbf{z}}_j$, distance between both agents as estimated by the ith vehicle
$\hat{\mathbf{z}}_j$	Position of jth agent as estimated by the ith vehicle
$\hat{\mathcal{Z}}_j$	Bounded region of uncertainty around the location of the jth vehicle
δ_{ij}	$\theta_i r_\epsilon / (\eta_i + \eta^c_j)$, time constant
Δ_{ij}	Bound on the localization error (i.e. uncertainty)
ϵ	A positive small constant
ϕ_i	Heading or orientation of ith vehicle
η_i	Enforced upper bound on the velocity of ith vehicle, $\|\dot{\mathbf{z}}_\mathbf{i}\| \leq \eta_i$
η^c_j	Upper bound on the velocity of jth agent's centroid, $\left\|\dot{\mathbf{z}}^c_\mathbf{j}\right\| \leq \eta^c_j$
κ_i	Design parameter for tracking control
$\bar{\mu}_i$	Upper bound of $\mathbf{u}_i$
θ_i	Design parameter
ρ_i	Wheels' radius
τ_i	Control torque input
$\tau_{\star i}$	Applied control torques at the left ($\star = L$) and right ($\star = R$) wheels
ω_i	Angular velocity of ith vehicle
ω_{ij}	$-(\eta_i + \eta^c_j)/r_\epsilon$
Ω_{ij}	ith vehicle's Avoidance region

Appendix B. Proof of Lemma 4.1

Proof. To simplify the notation, let $t_\delta = t_f - \delta_i$ and $\mathbf{z}_{ij}(t) = \mathbf{z}_i(t) - \mathbf{z}^c_j(t)$. From the assumption that $[\mathbf{z}^{\mathrm{T}}_i(t), \mathbf{z}^{c\mathrm{T}}_j(t)]^{\mathrm{T}} \in \mathcal{W}_{ij}\ \forall t \in [t_0, t_f]$, we have that $\mathbf{u}_i(t) = \mathbf{u}^a_i(t)\ \forall t \in [t_0, t_f]$ and, therefore, the velocity solutions for the ith vehicle at $t = t_f$ can be computed as $\dot{\mathbf{z}}_i(t_f) = e^{-k_i\delta_i}\dot{\mathbf{z}}_i(t_\delta) + \int_{t_\delta}^{t_f} e^{-k_i(t_f-\tau)}\mathbf{u}^a_i(\tau)\,d\tau$. Moreover, since $\|\dot{\mathbf{z}}_i(t_0)\| \leq \eta_i$, we can apply Lemma 2.2 and conclude that $\|\dot{\mathbf{z}}_i(t)\| \leq \eta_i\ \forall t \geq t_0$. Hence,

$$\begin{aligned}
\beta_{ij}(t_f) &= \mathbf{z}_{ij}(t_f)^{\mathrm{T}} e^{-k_i\delta_i}\dot{\mathbf{z}}_i(t_\delta) + \mathbf{z}_{ij}(t_f)^{\mathrm{T}} \int_{t_\delta}^{t_f} e^{-k_i(t_f-\tau)} \\
&\quad \bar{\mu}_i \frac{\hat{\mathbf{z}}_{ij}(\tau)}{\left\|\hat{\mathbf{z}}_{ij}(\tau)\right\|} d\tau \\
&\geq -\eta_i \left\|\mathbf{z}_{ij}(t_f)\right\| e^{-k_i\delta_i} + \bar{\mu}_i \left\|\mathbf{z}_{ij}(t_f)\right\| \\
&\quad \int_{t_\delta}^{t_f} e^{-k_i(t_f-\tau)} \frac{\mathbf{z}_{ij}(t_f)^{\mathrm{T}}\hat{\mathbf{z}}_{ij}(\tau)}{\left\|\mathbf{z}_{ij}(t_f)\right\|\left\|\hat{\mathbf{z}}_{ij}(\tau)\right\|} d\tau \\
&= -\eta_i \left\|\mathbf{z}_{ij}(t_f)\right\| e^{-k_i\delta_i} + \bar{\mu}_i \left\|\mathbf{z}_{ij}(t_f)\right\| \\
&\quad \int_{t_\delta}^{t_f} e^{-k_i(t_f-\tau)} \cos\phi_{ij}(\tau)\,d\tau
\end{aligned} \tag{25}$$

where $\phi_{ij}(\tau)$ defines the angle between $\mathbf{z}_{ij}(t_f)$ and $\hat{\mathbf{z}}_{ij}(\tau)$ for $\tau \in [t_\delta, t_f]$. Now, we will proceed to find a lower bound on $\int_{t_\delta}^{t_f} e^{-k_i(t_f-\tau)} \cos\phi_{ij}(\tau)\,d\tau$. In order to do so, we would like to define a function $\overline{\phi}_{ij}(\tau)$ such that $\phi_{ij}(\tau) \leq \overline{\phi}_{ij}(\tau)$ for all $\tau \in [t_\delta, t_f]$. Therefore, let us consider the diagram in Figure 17(a). Observe that $\phi_{ij}(\tau)$ is always upper bounded by the summation of the angle between $\mathbf{z}_{ij}(t_f)$ and $\mathbf{z}_{ij}(\tau)$ and the angle between $\mathbf{z}_{ij}(\tau)$ and $\hat{\mathbf{z}}_{ij}(\tau)$, denoted as $\vartheta_{ij}(\tau)$ and $\varphi_{ij}(\tau)$, respectively, i.e. $\left\|\phi_{ij}(\tau)\right\| \leq \left\|\vartheta_{ij}(\tau)\right\| + \left\|\varphi_{ij}(\tau)\right\|$. Hence, a suitable function would be

$$\overline{\phi}_{ij}(\tau) = \underbrace{\sup_{t\in[t_\delta,\tau]} \left\|\vartheta_{ij}(t)\right\|}_{\overline{\vartheta}_{ij}(\tau)} + \underbrace{\sup_{t\in[t_\delta,\tau]} \left\|\varphi_{ij}(t)\right\|}_{\overline{\varphi}_{ij}(\tau)}$$

where $\overline{\vartheta}_{ij}(\tau)$ and $\overline{\varphi}_{ij}(\tau)$ are yet to be determined.

Now, consider $\vartheta_{ij}(\tau)$. Since $\left\|\mathbf{z}_{ij}(\tau)\right\| \geq r_\epsilon\ \forall\ \tau \in [t_\delta, t_f]$ and the velocities of the agents are bounded, we have that $\vartheta_{ij}(\tau)$ attains its maximum when the agents approach each other at maximum speed along the boundary of Ω_ϵ, where $\Omega_\epsilon = \left\{\mathbf{z} : \mathbf{z} \in \Re^4, \left\|\mathbf{z}_{ij}\right\| < r_\epsilon\right\}$ (see Figure 17(b)

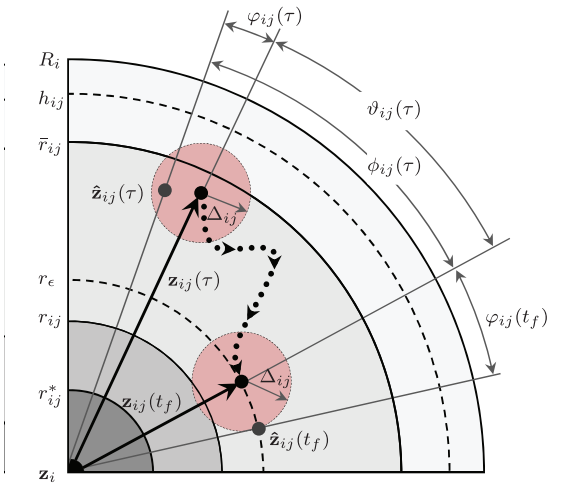

(a) Hypothetical motion of $\mathbf{z}_j(\tau)$ with respect to $\mathbf{z}_i(\tau)$ for $t_\delta \le \tau \le t_f$. The larger black dots represent the vectors (i.e. distances) $\mathbf{z}_{ij}(\tau)$ and $\mathbf{z}_{ij}(t_f)$, whereas the gray dots denote $\hat{\mathbf{z}}_{ij}(\tau)$ and $\hat{\mathbf{z}}_{ij}(t_f)$.

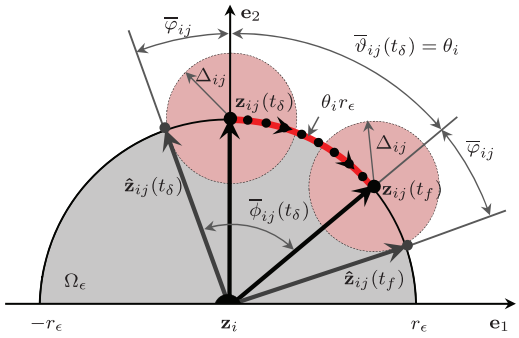

(b) Extreme case in Lemma 4.1. The agents approach each other at maximum speed along the boundary of Ω_ϵ.

Fig. 17. Geometrical interpretation of proof of Lemma 4.1.

for a pictorial representation). Then, using the arc-length formula, we can obtain that

$$\vartheta_{ij}(\tau) \le \frac{\int_\tau^{t_f} \left\| \dot{\hat{\mathbf{z}}}_{ij}(s) \right\| ds}{r_\epsilon} \le \frac{(\eta_i + \eta_j^c)(t_f - \tau)}{r_\epsilon} = \overline{\vartheta}_{ij}(\tau)$$

for $\tau \in [t_\delta, t_f]$. Note that $\overline{\vartheta}_{ij}(t_\delta) = \frac{(\eta_i + \eta_j^c)\delta_i}{r_\epsilon} = \theta_i$ while $\overline{\vartheta}_{ij}(t_f) = 0$. Now, we are left to find $\overline{\varphi}_{ij}(\tau)$.

Since $\left\| \mathbf{z}_{ij}(\tau) \right\| \ge r_\epsilon \ \forall\ \tau \in [t_\delta, t_f]$ and $\left\| \mathbf{d}_{ij} \right\| \le \Delta_{ij} < r_{ij}$, we have that $\varphi_{ij}(\tau)$ attains its maximum when $\mathbf{z}_{ij}(\tau)$ is close to the boundary of Ω_ϵ. Thus, let us once again consider the diagram in Figure 17(b). Observe that the maximum angle $\overline{\varphi}_{ij}(\tau)$ is constant whenever $\mathbf{z}_{ij}(\tau)$ lies on the boundary of Ω_ϵ. Consequently, it is sufficient to find $\overline{\varphi}_{ij}(\tau)$ when $\tau = t_\delta$. To this end, let us choose the vectors $\mathbf{e}_1$ and $\mathbf{e}_2$ as an orthonormal basis for the plane containing $\mathbf{z}_{ij}(t_\delta)$ and $\hat{\mathbf{z}}_{ij}(t_\delta)$, and let $\mathbf{e}_2$ be oriented along the same direction and origin as $\mathbf{z}_{ij}(t_\delta)$ (see Figure 17(b)). Then, $\mathbf{z}_{ij}(t_\delta)$ and $\hat{\mathbf{z}}_{ij}(t_\delta)$ can be rewritten as $\mathbf{z}_{ij}(t_\delta) = r_\epsilon \mathbf{e}_2$ and $\hat{\mathbf{z}}_{ij}(t_\delta) = c_1\mathbf{e}_1 + c_2\mathbf{e}_2$, where c_1 and c_2 are constants. Now, from the bound $\left\| \hat{\mathbf{z}}_{ij}(t_\delta) - \mathbf{z}_{ij}(t_\delta) \right\| = \left\| \mathbf{d}_{ij}(t) \right\| \le \Delta_{ij}$, we have that c_1 and c_2 must satisfy the equation: $c_1^2 + (c_2 - r_\epsilon)^2 \le \Delta_{ij}$. Likewise, we have that $\overline{\varphi}_{ij}$ is maximized when the ratio $|c_1/c_2|$ attains its maximum. Such conditions are satisfied when

$$c_1 = \pm \frac{\Delta_{ij}}{r_\epsilon}\sqrt{r_\epsilon^2 - \Delta_{ij}^2}, \qquad c_2 = \frac{r_\epsilon^2 - \Delta_{ij}^2}{r_\epsilon}$$

Therefore, $\overline{\varphi}_{ij}(\tau) = \overline{\varphi}_{ij}$ can be computed as

$$\overline{\varphi}_{ij} = \cos^{-1}\left(\frac{\mathbf{z}_{ij}(t_\delta)^{\mathrm{T}} \hat{\mathbf{z}}_{ij}(t_\delta)}{\left\| \mathbf{z}_{ij}(t_\delta) \right\| \left\| \hat{\mathbf{z}}_{ij}(t_\delta) \right\|} \right) = \cos^{-1}\left(\frac{\sqrt{r_\epsilon^2 - \Delta_{ij}^2}}{r_\epsilon} \right)$$

Now, returning to (25) and recalling that $\overline{\vartheta}_{ij}(\tau) \le \theta_i < \sin^{-1}\left(\frac{\sqrt{r_\epsilon^2 - \Delta_{ij}^2}}{r_\epsilon} \right)$, we have that $\overline{\phi}_{ij}(\tau) = \overline{\vartheta}_{ij}(\tau) + \overline{\varphi}_{ij}(\tau) < \frac{\pi}{2}$ and, therefore,

$$\begin{aligned} \int_{t_\delta}^{t_f} e^{-k_i(t_f-\tau)} \cos\phi_{ij}(\tau)\, d\tau &\ge \int_{t_\delta}^{t_f} e^{-k_i(t_f-\tau)} \cos\overline{\phi}_{ij}(\tau)\, d\tau \\ &= \frac{1}{k_i^2 + \omega_{ij}^2}\left(k_i \cos\overline{\phi}_{ij}(t_f) + \omega_{ij}\sin\overline{\phi}_{ij}(t_f) \right) \\ &\quad - \frac{e^{k_i\delta_i}}{k_i^2 + \omega_{ij}^2}\left(k_i \cos\overline{\phi}_{ij}(t_f) + \omega_{ij}\sin\overline{\phi}_{ij}(t_\delta) \right) \end{aligned} \tag{26}$$

where we used the fact that $\dot{\overline{\phi}}_{ij}(t) = \omega_{ij} = -\frac{\eta_i + \eta_j^c}{r_\epsilon}$ is constant. Also note that $\overline{\phi}_{ij}(t_f) = \overline{\varphi}_{ij}$ and hence

$$\begin{aligned} \cos\overline{\phi}_{ij}(t_f) &= \cos\overline{\varphi}_{ij} = \frac{\sqrt{r_\epsilon^2 - \Delta_{ij}^2}}{r_\epsilon} \\ \sin\overline{\phi}_{ij}(t_f) &= \sin\overline{\varphi}_{ij} = \frac{\left\| \mathbf{z}_{ij}(t_\delta) \times \hat{\mathbf{z}}_{ij}(t_\delta) \right\|}{\left\| \mathbf{z}_{ij}(t_\delta) \right\| \left\| \hat{\mathbf{z}}_{ij}(t_\delta) \right\|} = \frac{\Delta_{ij}}{r_\epsilon} \end{aligned} \tag{27}$$

To evaluate $\cos\overline{\phi}_{ij}(t_\delta)$ and $\sin\overline{\phi}_{ij}(t_\delta)$, let us rewrite $\mathbf{z}_{ij}(t_f)$ using $\mathbf{e}_1$ and $\mathbf{e}_2$ as orthonormal basis, i.e. $\mathbf{z}_{ij}(t_f) = r_\epsilon \sin\theta_i \mathbf{e}_1 + r_\epsilon \cos\theta_i \mathbf{e}_2$. Then, since $\overline{\phi}_{ij}(t_\delta)$ denotes the maximum admissible angle between $\hat{\mathbf{z}}_{ij}(t_\delta)$ and $\mathbf{z}_{ij}(t_f)$, we have that

$$\begin{aligned} \cos\overline{\phi}_{ij}(t_\delta) &= \frac{\sqrt{r_\epsilon^2 - \Delta_{ij}^2}\cos\theta_i - \Delta_{ij}\sin\theta_i}{r_\epsilon}, \\ \sin\overline{\phi}_{ij}(t_\delta) &= \frac{\sqrt{r_\epsilon^2 - \Delta_{ij}^2}\sin\theta_i + \Delta_{ij}\cos\theta_i}{r_\epsilon} \end{aligned} \tag{28}$$

and returning to (26), we obtain

$$\begin{aligned} \int_{t_\delta}^{t_f} e^{-k_i(t_f-\tau)} \cos\phi_{ij}(\tau)\, d\tau &\ge \frac{1}{r_\epsilon(k_i^2 + \omega_{ij}^2)} \\ &\Bigg(k_i\sqrt{r_\epsilon^2 - \Delta_{ij}^2} + \omega_{ij}\Delta_{ij} - e^{-k_i\delta_i}\omega_{ij}\sqrt{r_\epsilon^2 - \Delta_{ij}^2}\sin\theta_i \\ &\quad - e^{-k_i\delta_i}\omega_{ij}\Delta_{ij}\cos\theta_i \\ &\quad - e^{-k_i\delta_i}k_i\sqrt{r_\epsilon^2 - \Delta_{ij}^2}\cos\theta_i + e^{-k_i\delta_i}k_i\Delta_{ij}\sin\theta_i \Bigg) \end{aligned} \tag{29}$$

Finally, substituting the above equation into (25) verifies (19), and the proof is complete. □

Appendix C. Existence of solutions to the avoidance control problem

Theorem C.1. *A solution to Theorems 4.1 and 4.2 exists if, given a set of nonnegative parameters Δ_{ij}, η_i, η_j^c, $\bar{\mu}_i$, and θ_i and positive constant ϵ, the following inequality is satisfied*

$$R_i > \Delta_{ij} + (\theta_i + 1)\cdot \max\left\{r^*, \sqrt{\left(\frac{\alpha_i\sigma_i + \Delta_{ij}(1-\cos\theta_i)}{\sin\theta_i}\right)^2 + \Delta_{ij}^2} - \epsilon\right\} \quad (30)$$

where $\alpha_i = \eta_i(\eta_i + \eta_j^c)/\bar{\mu}_i$ and $\sigma_i = 1 + \frac{\eta_j^c}{\eta_i} e^{\frac{\theta_i(R_i-\Delta_{ij})}{\alpha_i}}$, if the problem is noncooperative, and $\sigma_i = 1$, otherwise.

Proof. In order to prove the above statement, we will compute an alternate sufficient condition to (21). To this end, let us consider the following inequality

$$\int_{t_\delta}^{t_f} e^{-k_i(t_f-\tau)} \cos\overline{\phi}_{ij}(\tau)\, d\tau \geq e^{-k_i\delta_i}\int_{t_\delta}^{t_f} \cos\overline{\phi}_{ij}(\tau)\, d\tau \quad (31)$$

which holds for $\overline{\phi}_{ij}(\tau) \geq 0$ and $\tau \in [t_\delta, t_f]$. From the proof in Lemma 4.1, we have that the left side of (31) is given by (29), while the right side can be computed as

$$e^{-k_i\delta_i}\int_{t_\delta}^{t_f} \cos\overline{\phi}_{ij}(\tau)\, d\tau = e^{-k_i\delta_i}\frac{\sqrt{r_\epsilon^2 - \Delta_{ij}^2}\sin\theta_i + \Delta_{ij}(\cos\theta_i - 1)}{\eta_i + \eta_j^c} \quad (32)$$

where we have used (27) and (28). Now, by substituting (29) and (32) into (31), we can demonstrate (after some manipulation) that the following inequality

$$\sqrt{r_\epsilon^2 - \Delta_{ij}^2}\sin\theta_i + \Delta_{ij}(\cos\theta_i - 1) - \alpha_i\sigma_i \geq 0 \quad (33)$$

is a conservative bound for (21). That is, if (33) holds, then (21) is satisfied. Now, suppose that (30) holds for the noncooperative or cooperative case, and choose r_{ij} as

$$r_{ij} = \max\left\{r_{ij}^*, \sqrt{\left(\frac{\alpha_i\sigma_i + \Delta_{ij}(1-\cos\theta_i)}{\sin\theta_i}\right)^2 + \Delta_{ij}^2} - \epsilon\right\} \quad (34)$$

which satisfies (20) in Theorems 4.1 and 4.2. Similarly, (34) satisfies (33), which in turn implies that (21) holds. Therefore, we conclude that if (30) holds for some given parameters Δ_{ij}, η_i, η_j^c, $\bar{\mu}_i$, ϵ, θ_i, and σ_i, then a solution to the avoidance problem exists. □